Tampere University

Leo Mäntynen

USE OF ALTERNATIVE BED MATERIALS TO INHIBIT BED AGGLOMERATION IN FLUIDIZED BED COMBUSTION OF BIOMASS FUELS

Faculty of Engineering and Natural Sciences
Master's Thesis
October 2020

ABSTRACT

Leo Mäntynen: Use of alternative bed materials to inhibit bed agglomeration in fluidized bed combustion of biomass fuels
Master's Thesis
Tampere University
Degree Programme in Environmental and Energy Engineering
October 2020

Bed agglomeration is a phenomenon, in which particles in a fluidized bed attach to each other and form larger clusters called agglomerates. It is a significant problem in fluidized bed combustion of certain biomass fuels that contain large amounts of alkali metals. Without countermeasures the agglomerates increase in number and size and may cause full defluidization, which refers to the collapse of the fluidized bed. This outcome necessitates boiler shutdown and leads to significant costs, which is why a lot of research is dedicated to the mechanisms and prevention of bed agglomeration.

The general consensus among researchers is that bed agglomeration is caused by an adhesive, silicate-dominated melt forming in the bed. Two main mechanisms of melt-formation have been recognized. In coating-induced agglomeration, bed particles are covered in ash, and chemical reactions in the ash coatings lead to melt formation. In melt-induced agglomeration, the melt is formed from ash without the presence of coatings. One possible way to prevent bed agglomeration is using quartz-free bed materials instead of natural sand. However, it is not clear how the usefulness of alternative bed materials is related to the different agglomeration mechanisms.

In this thesis, a literary review was conducted to summarize the current understanding of bed agglomeration mechanisms, its dependence on operational parameters, as well as methods to monitor and predict its occurrence. Additionally, combustion experiments were conducted in a lab-scale bubbling fluidized bed reactor to investigate the effect of fuel and bed material composition on agglomeration. Pine bark, tropical wood, oil palm empty fruit bunch (EFB) and wheat straw were used as fuels, while quartz, natural sand, GR Granule and olivine diabase were used as bed materials. The duration of each test was measured and bed samples were taken at regular intervals. The samples were analyzed using methods such as scanning electron microscopy and x-ray diffraction.

The results indicate that the benefits of using alternative bed materials depend on the composition of the fuel. Based on literature, tropical wood and pine bark were assumed to follow the coating-induced mechanism. For tropical wood, using alternative bed materials was effective. Defluidization was not achieved for bark, so bed materials could not be compared based on test durations. For EFB the choice of bed material did not affect agglomeration tendency, which could be explained by melt-induced agglomeration being the primary mechanism of agglomeration. Straw tests were unsuccessful, because of the excessive slagging of the reactor walls. Based on the test results and relevant literature, it seems that alternative bed materials are useful for fuels following the coating-induced agglomeration mechanism, but not for those obeying the melt-induced mechanism.

Keywords: bed agglomeration, fluidized bed combustion, biomass, alternative, quartz-free, bed material, defluidization

TIIVISTELMÄ

Leo Mäntynen: Vaihtoehtoisten petimateriaalien käyttö petiagglomeraation ehkäisyyn biomassan leijupetipoltossa
Diplomityö
Tampereen yliopisto
Ympäristö- ja energiatekniikan DI-tutkinto-ohjelma
Lokakuu 2020

Petiagglomeraatio on ilmiö, jossa leijupedin hiukkaset tarttuvat toisiinsa ja muodostavat isompia ryhmittymiä, joita kutsutaan agglomeraateiksi. Se on vakava ongelma silloin, kun poltetaan korkean alkalimetallipitoisuuden biomassapolttoaineita leijupetitekniikalla. Ilman ehkäiseviä toimenpiteitä, agglomeraatit kasvavat ja niiden määrä lisääntyy ja tuloksena voi olla leijupedin defluidisaatio, eli täysi romahtaminen. Tämä johtaa leijupetiprosessin alasajoon ja siten merkittäviin kustannuksiin. Siksi agglomeraatiomekanismien ja niiden ehkäisyn tutkimukseen on käytetty paljon resursseja.

Tutkijat ovat enimmäkseen yksimielisiä siitä, että petiagglomeraation aiheuttaa liimamainen, pääosin silikaateista koostuva sula aines petihiukkasten pinnalla. Kaksi päämekanismia on tunnistettu sulan muodostumiselle. Kerrosagglomeraatiossa (coating-induced agglomeration), petihiukkaset peittyvät tuhkakuoreen ja sula aines syntyy kuoren kerroksissa tapahtuvissa reaktioissa. Sula-agglomeraatiossa (melt-induced agglomeration) sula aines muodostuu tuhkasta ilman kuorikerrosten läsnäoloa. Yksi mahdollinen tapa agglomeraation ehkäisemiseksi on kvartsittomien petimateriaalien käyttö yleensä käytetyn luonnonhiekan sijaan. Ei ole kuitenkaan selvää, miten kvartsittomien petimateriaalien hyödyllisyys riippuu agglomeraatiomekanismista.

Tässä diplomityössä tehtiin kirjallisuusselvitys, jossa koottiin tämänhetkinen tieto agglomeraatiomekanismeista, eri prosessiparametrien vaikutuksesta ilmiöön ja tavoista, joilla agglomeraatiota voidaan ennakoida ja välttää. Lisäksi suoritettiin polttotestejä laboratoriokoon kuplivalla leijupetireaktorilla polttoaineen ja petimateriaalin koostumuksen vaikutuksen tutkimiseksi. Polttoaineina käytettiin männynkuorta, trooppista puuta, öljypalmun hedelmätertuista tehtyä pellettiä ja olkipellettiä. Petimateriaaleina toimivat puhdas kvartsi, luonnonhiekka, masuunikuona ja oliviinidiabaasi. Jokaisessa testissä mitattiin testin kesto ja petinäytteitä otettiin tasaisin väliajoin. Näytteitä tutkittiin käyttämällä erilaisia tekniikoita, kuten pyyhkäisyelektronimikroskooppia ja röntgendiffraktiota.

Tulokset viittaavat siihen, että vaihtoehtoisten petimateriaalien käytöstä saatu hyöty riippuu käytetystä polttoaineesta. Trooppisen puun ja männyn kuoren oletettiin kirjallisuuden perusteella noudattavan kerrosmekanismia. Trooppiselle puulle kvartsittomat petimateriaalit olivat tehokkaita agglomeraation ehkäisyssä. Defluidisaatiota ei tapahtunut männyn kuorella, joten petimateriaaleja ei voitu vertailla testien pituuden perusteella tällä polttoaineella. EFB:n poltossa käytetyllä petimateriaalilla ei ollut selvää vaikutusta agglomeraation etenemiseen, mikä viittaa siihen, että sulamekanismi oli vallitseva. Testit olkipelletillä epäonnistuivat, koska leijupetireaktorin seinät kuonaantuivat liikaa. Testituloksien ja kirjallisuuden perusteella vaikuttaa siltä, että kvartsittomat petimateriaalit ovat hyödyllisiä polttoaineille, joissa agglomeraatio aiheutuu pääasiassa kerrosmekanismista, mutta eivät niille, joilla sulamekanismi on hallitseva.

Avainsanat: petiagglomeraatio, leijupetipoltto, biomassa, vaihtoehtoinen, kvartsiton, petimateriaali, defluidisaatio

PREFACE

This Master's Thesis was written for Valmet Technologies Inc. in Tampere. The COVID-19 pandemic created somewhat exceptional circumstances for the work, as I did a large portion of the writing at home. Regardless of that, everything went smoothly because of the flexibility and professionalism of all parties involved.

First, I would like to thank Marko Palonen for recommending me to the position of thesis worker in the R & D function at Valmet technologies Inc. This great opportunity for thesis work would not have presented itself if not for his influence. I would also like to thank Sonja Enestam and all of the R & D Competences team for accepting me in their dynamic and creative group.

As for the thesis work itself, big thanks are due to the whole crew of Valmet R & D Center Tampere for help in various issues during the test runs and especially Tarmo Toivonen for his valuable advice on the operation of the Turre experimental reactor. A crucial part of the thesis was the analysis of the experimental samples, which was done by Satu Ilvonen at Eurofins Expert Services in Espoo. I am very thankful for her for answering all the questions and additional analysis requests I had after the first report. Many thanks also to Tapio Klasila from the same company for sharing his expertise on bed agglomeration.

The biggest thanks inevitably go to Jaakko Tamminen, who acted as a supervisor on the Valmet side of the project. Jaakko had an integral part in the thesis work, since he lead the experimental campaign and arranged the operational data acquired from the tests. He also gave valuable feedback on the theory part in its different stages. Jaakko's professional intelligence and friendly personality make working with him very enjoyable and cooperation effortless.

Furthermore, I am very grateful to my examiner and supervisor, professor Jukka Konttinen from the Faculty of Engineering and Natural Sciences at Tampere University. He let me work independently, but still offered useful comments at numerous occasions.

I would also like to extend thanks to all my friends for all the next-level humorousness that their company has provided. Finally, I would like to thank my mum, dad and brother for their continued support throughout my life.

Tampere, 6th October 2020

Leo Mäntynen

CONTENTS

LIST OF ABBREVIATIONS

BE	backscatter electron
BFB	bubbling fluidized bed
BFS	blast furnace slag
CFB	circulating fluidized bed
CFBA	controlled fluidized bed agglomeration
CFD	computational fluid dynamics
DDPM	dense discrete phase model
DEM	discrete element method
EDS	energy-dispersive x-ray spectroscopy
EFB	empty fruit bunch
EU	European Union
FBC	fluidized bed combustion
GRG	GR Granule
MSW	municipal solid waste
PVC	polyvinyl chloride
RDF	refuse-derived fuel
RMSE	root-mean-square error
SEM	scanning electron microscopy
SRF	secondary recovered fuel
XRD	x-ray diffraction
XRF	x-ray fluorescence

LIST OF SYMBOLS

$\mathbf{Ca}$	capillary number	$-$
$\mathbf{F_c}$	capillary force	$\mathbf{N}$
$\mathbf{F_d}$	viscous dissipation force	$\mathbf{N}$
$\mathbf{n}$	number of predictions	$-$
$\mathbf{U}$	fluidizing gas velocity	$\mathbf{m/s}$
$\mathbf{U_{mf}}$	minimum fluidization velocity	$\mathbf{m/s}$
$\mathbf{v_{rel}}$	relative velocity of colliding particles	$\mathbf{m/s}$
γ	surface tension	$\mathbf{N/m}$
μ	viscosity	$\mathbf{Pa \cdot s}$
θ	observed value of the variable being predicted	
$\hat{\theta}$	model value	

1 INTRODUCTION

The projected consequences of global warming include sea level rise, loss of biodiversity and increase in extreme weather phenomena. Significant reductions in the global greenhouse gas emissions are required in order to lower the environmental and economical risks associated with these changes. [53, p. 7–12] Heat and power production is the single largest source of anthropogenic greenhouse gas emissions, with a share of about 30 % [20]. Therefore, it makes sense to look for ways to substitute fossil fuels in the energy sector with potentially carbon neutral alternatives, like *biomass* [103, p. 10].

Plants capture CO_2 from the atmosphere during their growth. When a plant dies, the stored energy in the biomass is released in an oxidation reaction and the fixed carbon is released as carbon dioxide. This process can happen either slowly by decomposition or fast in a forest fire. In biomass combustion applications, this natural reaction is moved inside a boiler, in which the energy can be recovered and used to produce steam, heat and electricity. [1, p. 54] Thus, the combustion of plant biomass can be considered carbon neutral, when regulated cultivation methods are followed. The same idea of release of greenhouse gases during decomposition is true for waste biomass. [103, p. 40]

However, biomass fuels have some properties that make them challenging to burn. The most significant issues are caused by the composition of the *ash-forming matter* in these fuels. Some chemical elements, such as alkali metals and chlorine, promote *fouling* and *slagging* on the cold surfaces of boilers, resulting in reduced heat transfer and *corrosion* [85, p. 284][70, p. 155]. The ideal technology for handling these problems is *fluidized bed combustion (FBC)* [108, p. 212].

Unfortunately, the combustion of low-grade biomass fuels in fluidized bed boilers may lead to *bed agglomeration*. Bed agglomeration is a phenomenon, in which bed particles in a fluidized bed attach to each other and form larger structures called *agglomerates* [12, p. 634]. Bed agglomeration is exploited in many industries to create solid pieces from powdery matter through the use of wet granulation [28, p. 1868]. In FBC however, bed agglomeration is a significant problem.

Bed agglomeration affects the hydrodynamic behaviour of the fluidized bed in a way that could lead to temperature peaks and an increase in generation of secondary pollutants [108, p. 224–225]. Without countermeasures, the agglomerates increase in number and size until the air can no longer hold them afloat, resulting in *defluidization*. Full defluidization necessitates a plant shutdown. The bed must be cooled and the agglomerated

particles need to be replaced with fresh material. This leads to financial losses, that could endanger the profitability of the plant. [72, p. 453] Moreover, additional plant start-up and shut-down cycles could shorten the working lifespan of the equipment [65, p. 38–42]. As a consequence, significant effort is put in the research of mechanisms, detection and prevention of bed agglomeration [72, p. 453][12].

One possible way to avoid bed agglomeration is the use of *alternative bed materials* that do not contain quartz [12, p. 660–661]. However, there is evidence in the literature that quartz-free bed materials are not useful for all fuels [12, p. 660–661][45, p. 4558][122, p. 4537–4539][30, p. 2666]. More research is needed on the effect alternative bed materials have on different agglomeration mechanisms.

The main research questions of this thesis were the following:

- *What mechanisms cause bed agglomeration?*
- *How are agglomeration mechanisms affected by changes in operational parameters like fuel and bed material composition? Specifically, what are the agglomeration tendencies of pine bark, tropical wood, oil palm empty fruit bunch and wheat straw? What is the difference between using quartz, natural sand, GR Granule and olivine-diabase as bed material?*
- *What methods are available for predicting agglomeration and monitoring its occurrence in fluidized bed boilers?*

This thesis is structured as follows. First, chapter 2 introduces biomass as a fuel and fluidized bed combustion as a technology, with a focus on the ash-related issues encountered with biomass fuels. Chapters 3, 4 and 5 review the current understanding of bed agglomeration mechanisms, their relationship to different operational parameters, as well as monitoring and prediction of bed agglomeration. Chapter 6 presents the experimental reactor, analysis methods, fuels and bed materials used in the agglomeration test runs. The results of these experiments and their implications are discussed in Chapter 7. Finally, the entire work is summarized in chapter 8 and suggestions for further research are given.

2 FLUIDIZED BED COMBUSTION OF BIOMASS FUELS

The use of biomass fuels as alternatives for fossil fuels is increasing due to their widely accepted carbon neutrality, relatively cheap prices and good availability [108, p. 19–20][111, p. 378]. On the other hand, biomass utilization is connected with multiple technical problems. Many of the issues can be reduced by using fluidized bed combustion, which has become the main combustion technology for biomass-fired boilers larger than 50 MW_{th}. [108, p. 212] Nevertheless, some obstacles still remain for the use of the more difficult types of biomass [12, p. 634].

2.1 Biomass as a fuel

Biomass is defined as biological material from living or dead organisms [108, p. 22]. The distinction between biomass and fossil fuels is made by speed of regeneration and begins with peat, which is not considered a type of biomass. Some definitions separate waste fuels into their own category, while others include them in the group of biomass fuels. The latter view is used in this thesis. In addition to plants and animals, biomass includes all their wastes and residues, organic waste from households and trade, as well as various products and wastes from industries using biomass as raw material. [103, p. 29][54, p. 26][108, p. 20] Many of these materials have properties that are challenging from the standpoint of combustion [103, p. 43–49].

2.1.1 Categorization

Biomass fuels can be categorized in several ways [58, p. 6–7][108, p. 22][44][54, p. 21, 26]. One fundamental distinction can be made between *residual or waste biomass* and *energy crops*. Residual biomass comprises residues from agriculture and forestry, as well as organic parts of wastes from households and industry. On the other hand, energy crop is a term used for plants grown exclusively for energy conversion. [103, p. 30] For the purp oses of this thesis, the origin of the biomass is not as important as the composition. Therefore, both residual biomass and energy crops are included into the following three groups: *wood-derived fuels*, *agricultural fuels* and *waste fuels* [54, p. 21, 26][126, p. 6372–6375][90].

Wood-derived fuels include fuels consisting of different parts of trees, residues from wood

harvesting and processing as well as used wood from biomass-derived products [44, p. 23–24]. Wood-derived biomass accounts for about 80 % of biomass feedstocks used for heat and power production in the world [52, p. 216–217]. In industrial countries, trunk wood is normally used by the wood processing industry and a large fraction of the wood-derived fuel in energy conversion consists of residual wood [103, p. 29][108, p. 19][90]. Some fast-growing trees, such as willows and poplars, are used as energy crops [47, p. 9–10].

The category of agricultural fuels in this thesis includes both herbaceous and fruit biomass. Herbaceous fuels include straws, grasses, leaves and other annual growth materials [54, p. 25–26]. The EU standard EN 14961-1 incorporates different parts of cereal crops, grasses, oil seed crops, root crops, legume crops and flowers in this group. Fruit biomass includes parts of fruit-bearing plants and nuts. [44, p. 25, 27] Agricultural byproducts commonly used as fuel include bagasse, pressing residues, husks, shells and kernels. Animal manure from livestock can also be included in the category of agricultural biomass fuels. As for agricultural energy crops, conventional cereals could be used for this purpose, but ethical and moral concerns have been raised about the use of crops that could also be used as food. [103, p. 30–32][90] Non-edible grass-type energy crops include *Miscanthus*, switchgrass and reeds [47, p. 9–10].

Waste fuels include *municipal solid waste (MSW)*, *industrial waste*, *refuse-derived fuel (RDF)*, *secondary recovered fuel (SRF)*, *sewage sludge* and other types of combustible waste [103, p. 37–38][54, p. 26][90][121, p. 605]. MSW refers to combustible waste collected from households. The biogenic fraction in it may consist of paper, cardboard, wood, food, leather, textiles and yard trimmings. Industrial wastes considered as organic may originate from wood, pulp and paper, textile and food industries. [90] In Europe, municipal, industrial and residual wastes are often pretreated into RDF or SRF to improve the combustion properties. Another waste fuel, sewage sludge, refers to the residual material from treatment of household and industrial wastewaters. [103, p. 37–38]

2.1.2 Fuel characteristics

Due to the fact that biomass encompasses so many different materials, the fuel characteristics may vary greatly between different fuels in the same category [59, p. 23]. Some of the more general properties are discussed below.

Biomass fuels, especially those from agricultural origin, typically have low *bulk densities*. For example, brown coals can have a density of 740 kg/m^3 [103, p. 49], while for straw the corresponding value is in the range of 30–40 kg/m^3 [1, p. 131]. Low density leads to relatively low volumetric heating values, process control difficulties, larger storage requirement, expensive transportation and limitation in available technologies. Densification techniques such as baling, briquetting and pelletization can be used to raise the density of biomass fuels, but they come with added energy requirement and cost. [59, p. 25]

Another important fuel property is *moisture content*, which is typically higher for biomass than for coal. Fresh wood, for example, contains between 40 to 60 % moisture [103, p. 43]. High moisture content leads to a high volume of the flue gas produced; therefore, larger equipment is required [59, p. 26]. Moisture content is strongly connected to *heating value*, which is the standard measure for energy content in a fuel [54, p. 36]. In general, the more a fuel contains carbon and hydrogen, the larger is its heating value [1, p. 56]. In biomass, the fraction of these elements is typically lower than in fossil fuels. This in combination with high moisture content leads to low heating values. [59, p. 26] The dry lower heating values of most biomass fuels fall in the range of 10–20 MJ/kg [121, p. 605][1], when for bitumic coals the value is closer to 30 MJ/kg [1, p. 173]. For wastes the organic fraction typically has a relatively low heating value compared to paper and plastic materials [103, p. 49].

In general, biomass fuels contain a large amount of *volatile compounds*, which is why they burn with a long flame and require a large combustion space. Whereas antracite coals normally lose less than 10 % of their mass during pyrolysis, for biomass the same value is often about 75 %. [54, p. 27][1, p. 54]

Biomass fuels also differ from other solid fuels by the behaviour of their ash. A significant portion of the ash-forming matter in biomass is typically released as inorganic vapors. Some biomasses also have a large fraction of ash-forming elements and a low ash melting temperature. [111, p. 379–386][54, p. 27–28] The ash compounds can participate in many undesirable reactions in the furnace. The ideal technology to control these difficulties is *fluidized bed combustion* [108, p. 212].

2.2 Fluidized bed combustion

Since the 1930s, fluidized bed reactors have been used in petrochemistry and coal gasification. The first commercial systems for combustion of solid fuels were introduced in the 1970s. In Scandinavia, fluidized bed boilers were at first used to fire biomass, while in North America they were used for bituminous coal. Today, fluidized bed combustion is a widely accepted technology for the combustion of different solid fuels. [108, p. 211–212][85, p. 490]

2.2.1 Theory of fluidized beds

In fluidized bed technologies, an evenly distributed stream of gas is blown upwards through a layer of bed material particles. With a sufficiently high gas velocity, this gas-solid system exhibits liquid-like properties and is called a fluidized bed. [61, p. 1]. Figure 2.1 shows *the fluidization regimes* that are used to classify bed properties with different fluidizing gas velocities [85, p. 491–492].

If the gas velocity is low, the drag force acting on the particles is not large enough to overcome their weight. This condition is called *a fixed bed*. When gas flow is increased,

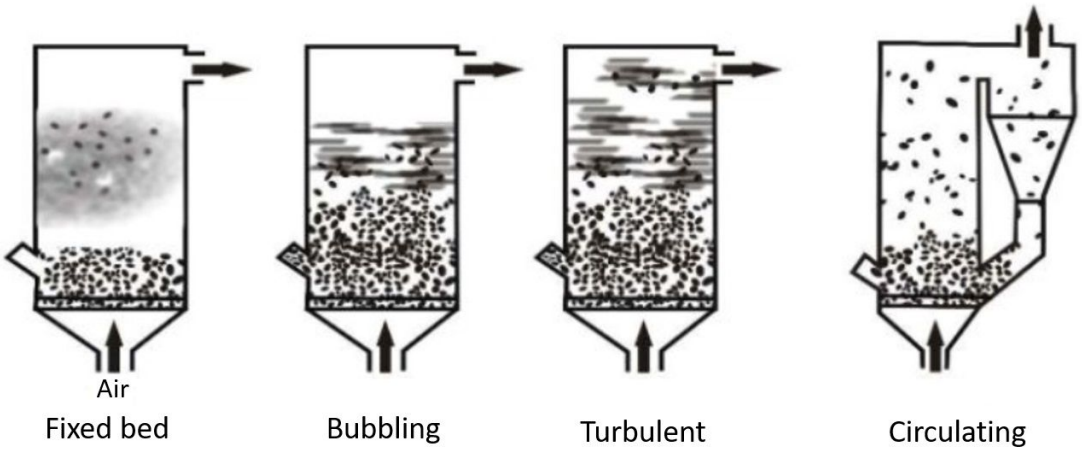

Figure 2.1. *Fluidization regimes [86, p. 1].*

the drag force will eventually balance the gravitational force on the particles and they become suspended in the gas stream. At this point the gas velocity is called *the minimum fluidization velocity*. [85, p. 491][61, p. 1–2]

Further increase in the gas flow will lead to *the bubbling regime*, where bubbles start to form in the bed and it becomes less uniform. The volume of the bed increases significantly, but there is still a clear boundary between the bed and the space above it. In *the turbulent regime* the gas flow approaches the terminal velocity of the particles. The bubbles grow larger and start to coalesce, forming larger voids in the bed. The bed particles form interconnected groups of high solids concentrations and the bed surface is not as distinct anymore. If the gas flow is increased even further, the particles are blown out of the bed and the container. This regime is called *pneumatic transport*. In order to keep the particles in the system, they must be separated from the gas and circulated back to the bed, as shown in the rightmost image in figure 2.1. [85, p. 491–492]

The minimum fluidization velocity depends on many parameters, such as the size and density of the bed particles, particle shape, gas viscosity and bed void fraction. Void fraction refers to the fraction of the furnace occupied by gas. [108, p. 213–214][85, p. 496] The particle sizes in fluidized bed applications usually vary from 0.015 to 6 mm. Geldart [41] has classified the types of fluidization behaviour based on the particle size of the bed material and the density difference between bed material and fluidization gas. Figure 2.2 shows the Geldart particle classification diagram. [85, p. 492–494]

The Geldart groups have the following properties in the order of increasing particle size. Group C is the fluidization behaviour observed for very fine particles with diameters less than 20 µm [91, p. 68]. For this group, fluidization is extremely difficult, because of the electrostatic and other interparticle forces acting between particles. For group A particles the fluidization state is achieved relatively easily, but bubbling starts only when the minimum fluidization velocity is exceeded significantly. Group B is the fluidization state encountered with sand. Fluidization is typically achieved with particles sizes from 50 to 500 µm and densities of 1400–4000 kg/m^3. Bubble formation starts immediately after

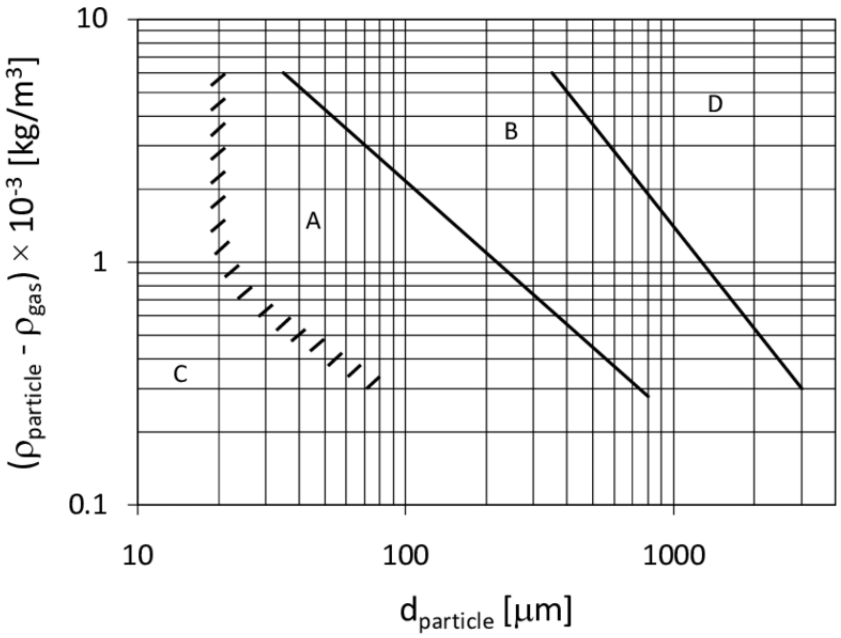

Figure 2.2. *Geldart powder classification diagram for fluidization by air [33, p. 13], original from [41, p. 290].*

the minimum fluidization velocity is exceeded and fluidization is efficient. Fluidization of large particles ($>$1 mm) exhibit the behaviour of group D. In this case the required fluidization gas velocity is considerably high. Bubbles can fill the whole cross section of the fluidization space, leading to a pulsating fluidization state, which is difficult to control. [85, p. 494]

2.2.2 Fluidized bed combustion technologies

In *fluidized bed combustion (FBC)*, air is used as the fluidization gas and the most common bed material is *natural sand* [51, p. 8]. Solid fuel is mixed with the hot sand bed in the furnace to promote combustion [108, p. 213]. Figure 2.3 shows a simplified cross-sectional diagram of the two main technologies used in FBC applications.

Bubbling fluidized bed (BFB) systems (figure 2.3 a) usually operate in the bubbling fluidization regime with Geldart type B particles. The boiler construction is relatively simple and consists of a furnace with a rectangular cross-section and a backpass, through which flue gases are led out of the process. Typically only half of the combustion air is supplied through the bottom plate and the rest above the bed to control NO_x emissions by air staging. [85, p. 500][108, p. 217]

Circulating fluidized bed (CFB) boilers (figure 2.3 b) operate between the turbulent and pneumatic transport regimes. The bed particle size is typically lower than 0.5 mm. A cyclone is used to separate the entrained bed particles from the flue gas. Collected particles are reinjected to the lower part of the furnace via a loop seal. [85, p. 490, 493, 517][108, p. 222, 228–229]

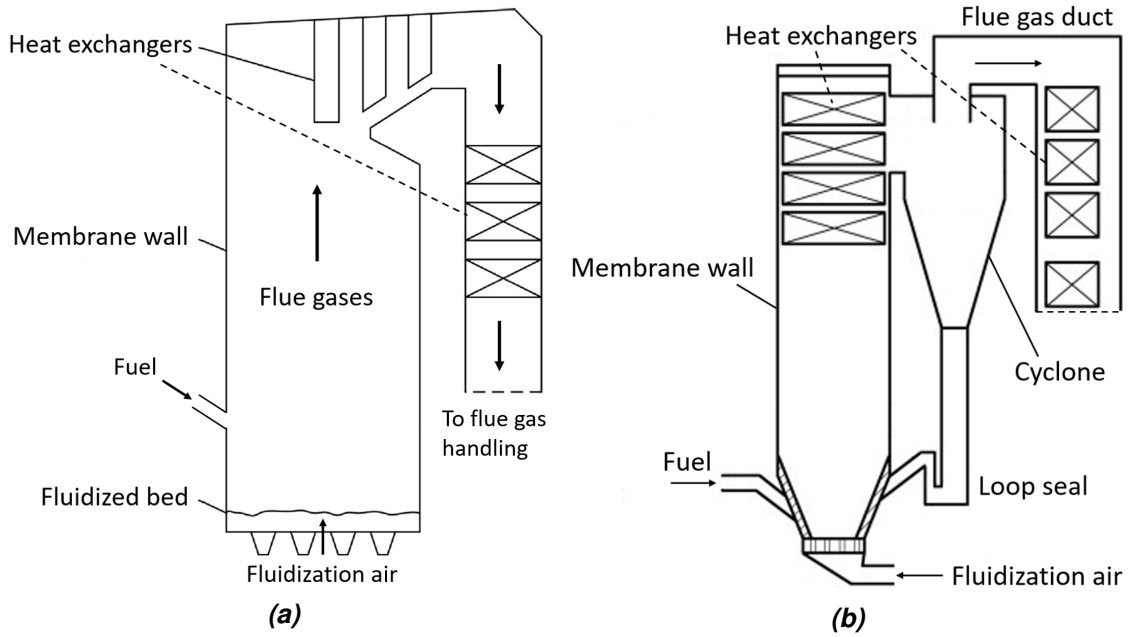

Figure 2.3. *Example cross-sectional geometries of the (a) BFB and (b) CFB. Edited from [72, p. 454] and [127, p. 102].*

The basic principle of steam generation in both technologies is the same. The fluidized bed is first heated by oil- or gas-fired startup burners. When the fuel feeding is started, the hot sand particles will facilitate combustion. [108, p. 213, 219] Fluidized bed boilers typically operate in the temperature range of 750–900 °C [85, p. 490]. The furnace walls are made of welded tubes forming a so-called *membrane wall*. Inside the tubes, water is evaporated by the heat released by combustion reactions. From there the wet steam is transported to different locations in the boiler, where it absorbs more heat from the flue gases. The location and amount of the heat exchanger surfaces will depend on the boiler type, fuel and desired steam parameters. [108, p. 219, 222]

Carrying out combustion in a fluidized bed has numerous benefits compared to other combustion technologies. The thermal capacity of the bed enables fast fuel drying and a relatively constant temperature, even if the quality of the fuel varies. This leads to a high combustion efficiency, allowing the use of fuel mixtures and fuels with challenging properties, like high moisture content. NO_x emissions from fluidized bed boilers are low and sulfur removal can be arranged relatively easily by injecting limestone into the furnace. [108, p. 212–213][85, p. 490]

Compared to CFB boilers, BFB boilers are cheaper owing to their simple construction and can be used for fuels with a higher moisture content. They also consume less energy during operation. CFB boilers can be used for a wider range of fuels, they have lower NO_x and SO_x emissions and a higher combustion efficiency in coal combustion. Typically BFB boilers are used in applications of less than 100 MW_{th} and CFB boilers from 50 MW_{el} upwards. [85, p. 490–491][108, p. 212][32]

FBC technologies are effective for controlling the issues arising from difficult ash-forming

element compositions and low ash melting temperatures, since they operate at a low steady temperature and are not very sensitive to variations in fuel composition [108, p. 212]. However, not all ash-related technical difficulties in FBC have been solved.

2.3 Ash-related problems in fluidized bed combustion of biomass

Biomass fuels have a broad range of concentrations of different ash-forming compounds. Significant variation can be observed not only between the biomass types, but also within the specific species and even between different parts of a single plant [1, p. 57–58][111]. The most important chemical elements in biomass ash are Si, Ca, Mg, K, Na, P, Al, S and Cl. [14, p. 86] In some waste fuels, Zn and Pb may also be present in considerable amounts [67, p. 130].

During combustion, ash compounds are released to the flue gas and go through a complicated chain of chemical reactions. The final form of the given ash element will depend on its original association in the fuel, as well as the furnace conditions. [126, p. 6380][14, p. 86–89] Some of the chemical reactions can lead to formation of a molten phase, which causes ash particles to become adhesive. The adhesive ash can cause operational problems in different parts of the boiler, including *fouling*, *corrosion*, *slagging* and *bed agglomeration*. Ash-related issues are the most common reason for unplanned shutdowns of commercial boilers [85, p. 269].

2.3.1 Ash-forming element composition in different biomasses

Elemental composition is determined from fuel ash after a standard ashing procedure. A common practise is to give the fraction of each ash element as if they were present as their most common oxides. This assumption is rarely true, but it usually gives a good estimation of the amount of oxygen in the ash. As highly volatile elements, chloride and sulfur are often excluded from this method. [51, p. 4–5][16, p. 826][30, p. 2664] The elemental ash composition is not the whole truth, since a given ash-forming element can be present as a part of many different compounds. These compounds could be identified from the fuel based on their solubility, like in chemical fractionation. [126, p. 6369]

The ash-forming compounds can be classified into four general groups [126, p. 6368][87, p. 159]. *Organically bound matter* denotes metal ions bound to anionic groups in the organic molecules that constitute the biomass. *Dissolved salts* consist of metal cations and small, often inorganic anions that have been dissolved in the fluids of the plant. These salts will precipitate if the biomass is dried, but will remain in soluble form. *Included minerals* are minerals precipitated in biomass as a result of natural processes. They are incorporated in the carbonaceous material of the fuel. *Excluded mineral matter* refers to compounds originating from impurities mixed in the fuel during growth, harvesting and

processing, as well as waste-derived foreign matter, such as polyvinyl chloride (PVC), metallic aluminium, Pb, Zn or Cu. Excluded minerals are probably significantly less reactive than included minerals [14, p. 86].

Table 2.1 shows the amount and composition of ash-forming elements for four example fuels.

Table 2.1. *Inorganic element compositions in different fuels [111][81].*

	Wood fuel **Pine bark**	**Agricultural fuel 1** **Wheat straw**	**Agricultural fuel 2** **Rapeseed cake**	**Waste fuel** **MSW**
Inorganic elements, (wt–% of dry matter)				
Total ash	1.7	7.9	7.5	47.2
Cl	0.01	6.01	0.7	7.8
S	0.02	0.12	0.5	0.70
Ash composition as oxides (wt–% of ash)				
SiO_2	9.20	52.56	1.43	37.92
CaO	56.83	8.03	14.74	24.66
MgO	6.19	2.67	9.29	3.82
K_2O	7.78	23.07	20.24	4.79
Na_2O	1.97	3.80	8.09	6.34
P_2O_5	5.02	3.28	39.42	0.74
Al_2O_3	7.20	1.78	0.25	13.62

Wood-derived fuels, such as bark, typically have a low inherent ash content, often less than 1 wt–% of dry matter. The main ash-forming elements are Ca and K. Higher ash content and substantial Si and Al concentrations typically result from contamination with excluded mineral matter. Waste wood is an exception in the category of wood-derived fuels and its composition can vary in a wide range. Waste wood can contain significant amounts of waste-derived elements, such as Na, Pb, Zn and Ti. [111, p. 395][126, p. 6372–6373]

Agricultural fuels are a diverse group with a wide range of ash properties [126, p. 6374]. The ash content is typically considerably higher than in wood-derived fuels [14, p. 90]. Straws, for example, normally contain between 2.8–8.8 wt–% of ash [126, p. 6374]. The primary ash-forming elements in agricultural biomass fuels are Si, K and Ca [111, p. 387]. As opposed to woody biomass, in many agricultural fuels Si is integrated to the organic structure of the fuel. Some agricultural fuels also have high Cl, S or P content. [126, p. 6374–6375, 6380] Rapeseed cake, [81, p. 2031–2032][46, p. 939] cereal grains [68] and chicken manure [117, p. 546] are examples of phosphorus-rich agricultural fuels.

Waste fuels also have highly variable ash compositions. The ash content is often very high: for example, MSW and sewage sludge may contain about 50 wt–% of ash [111, p. 385][126, p. 6375]. On average, the most common inorganic elements in waste fuels are Si, Ca and Al [111, p. 388]. Sewage sludge may contain significant amounts of P and Fe,

when $Fe_2(SO_4)_3$ is used in wastewater treatment as a precipitating agent for phosphates [126, p. 6375].

2.3.2 Release and transformation of ash-forming matter

The specific reaction path of ash-forming matter varies based on the physical environment inside and around fuel particles, and can be very different between two processes [14, p. 86]. This section provides a summary of the behaviour of the most important ash elements in the furnace. More comprehensive descriptions can be found from Boström et al. [14] and Zevenhoven et al. [126, p. 6380–6382].

Silicon can be present in biomass ash as *quartz*, which is one of the crystalline forms of *silica* (SiO_2), and other excluded mineral matter, such as *silicate minerals* that contain metals like K, Na, Ca and Al [22, p. 108][126, p. 6368]. These solid materials usually have high melting point temperatures and will not cause problems on their own. However, they might participate in reactions with alkali and alkaline earth metals in the furnace. These reactions could modify the composition of the silicates into a low melting point region, while also binding some of the ash-forming matter to these materials. Examples include reactions of alkali metal vapors with quartz, written as [126, p. 6380–6381][51, p. 8]

$$\mathrm{SiO_2\,(s) + K_2CO_3\,(g) \longleftrightarrow K_2SiO_3\,(s,l) + CO_2\,(g)}, \tag{2.1}$$

$$\mathrm{SiO_2\,(s) + 2\,KCl\,(g) + H_2O\,(g) \longleftrightarrow K_2SiO_3\,(s) + 2\,HCl\,(g)\ and} \tag{2.2}$$

$$\mathrm{SiO_2\,(s) + 2\,KOH\,(g) \longleftrightarrow K_2SiO_3\,(s) + H_2O\,(g)}. \tag{2.3}$$

Silicon can also occur in plants as included, amorphous mineral SiO_2 (phytoliths) or a dissolved salt $Si(OH)_4$ (aq). These types of silicates will probably be released as small SiO_2 (s) particles during combustion [14, p. 86–87]. The sources do not specify are these released particles quartz or some type of amorphous silica. According to Zevenhoven et al. [126, p. 6380], the organic structure of some agricultural fuels contains finely distributed Si and K in nearly equal concentrations. For example in straw, up to 5 % of the silicon occurs near potassium and is soluble in water. These reactive silicates can react with each other during combustion and form low melting point potassium silicates.

Potassium is the most important ash-forming element in regards to ash-related problems in biomass combustion. Potassium is mainly present in a soluble form, either as cations in dissolved salts, or organically bound in carboxylic groups. The potassium in these forms is released during combustion and can take part in various chemical reactions in the flue gases. Sodium is often grouped together with potassium, since its chemistry is similar and its concentration in biomass is normally an order of magnitude lower. [126, p. 6381–6382][14, p. 86]

In the first stage of the reactions involving potassium, K (g), KOH (g) and corrosive KCl (g) are formed in different fractions depending on the amount of oxygen and chlorine available in the furnace. These compounds undergo further reactions, again depending on the specific conditions. When no sulfur or phosphates are present, KCl (g) condenses as aerosol particles or on the surface of the ash. K (g) and KOH (g) may condense as carbonate particles. In the presence of sulfur, the alkali species will participate in *sulfation* reactions. Sulfation begins with reactions of SO_2 and SO_3 with KCl or KOH, producing $KHSO_4$ or KSO_3Cl. [42][126, p. 6381][14, p. 87–88] These gases may react further according to the equations

$$\mathrm{KSO_3Cl\,(g) + H_2O\,(g) \longleftrightarrow KHSO_4\,(g) + HCl\,(g)\,and} \tag{2.4}$$

$$\mathrm{KHSO_4\,(g) + KCl\,(g) \longleftrightarrow K_2SO_4\,(g) + HCl\,(g).} \tag{2.5}$$

Calcium is the main ash-forming element in wood-derived biomass. It occurs in organically bound forms as well as crystalline salt particles [125, p. 507]. Calcium is released as fine solid CaO particles that are highly reactive. The most important reactions include sulfation and *recarbonation*. [126, p. 6382][14, p. 87] Sulfation removes SO_2 from the process through the reaction

$$\mathrm{CaO\,(s) + SO_2\,(g) + \frac{1}{2}\,O_2\,(g) \longleftrightarrow CaSO_4\,(s).} \tag{2.6}$$

As a consequence, less sulfur dioxide is available to participate in other reactions, such as sulfation of alkali chlorides. The recarbonation of CaO can be written as

$$\mathrm{CaO\,(s) + CO_2\,(g) \longleftrightarrow CaCO_3\,(s).} \tag{2.7}$$

Magnesium is also present in many biomasses, but usually in significantly lower concentrations than calcium. Its chemistry is similar to that of calcium, but in most cases relevant to FBC, it is much less reactive. [126, p. 6382]

Sulfur can occur in biomass as inorganic sulfate ions or organic S. In woody biomass, about 75 % of the sulfur is organically bound. Organic sulfur will be fully released in the fuel gas as compounds that ultimately react to form SO_2. It is not clear what happens to the inorganic alkali sulfates. They could either stay in compound form or decompose, releasing the S. In sewage sludges, S may originate from waste processing chemicals that also decompose into the final product SO_2. Depending on the oxygen concentration, SO_2 will later oxidize to SO_3. The chemistry of sulfur has a significant effect on other furnace reactions, such as the ones involving potassium. [126, p. 6382][124, p. 9]

Chlorine occurs in biomass as chloride salts. Some portion of the elemental Cl could also be bound in organic chlorine compounds, such as residues of PVC found in waste-

derived fuels. Chlorine is usually fully released from the fuel as chloride vapors NaCl, KCl, $ZnCl_2$ and $PbCl_2$ or gaseous HCl. The chlorides may further react with other ash-forming compounds in various different reactions. [126, p. 6382]

Phosphorus in biomass fuels can be present as soluble *phosphate* salts or as part of organic molecules. The ratio of inorganic and organic phosphorus varies for different types of biomass. During combustion, phosphorus is probably released as P_4O_{10} (g) and may form alkali and alkaline earth phosphates. When phosphate anions are present, metal cations will more likely form phosphates than silicates. [126, p. 6383][14, p. 87–88][46, p. 946]

Aluminium in biomass fuels can take many different forms. Organically bound Al and precipitated Al-salts will form alumina (Al_2O_3) during combustion. It is a seemingly inert compound. Aluminosilicates can end up in biomass from impurities such as clay and they are sometimes also used as bed materials. They may react with alkali vapors, but are not very reactive. In some waste-derived fuels, metallic aluminium Al (s) or aluminium sulfates can be found and they will usually oxidize to alumina. In sewage sludge, aluminium may be present as zeolites, which influence the alkali chemistry in boilers in the same way as other silicate minerals. [126, p. 6381]

2.3.3 Ash melting

Some biomass ash compounds can form a melt in the temperature range used in FBC [72, p. 461]. Even if the melting temperature of separate constituents is higher, as a mixture or a compound they may form melt at a lower temperature. These types of mixtures do not have a single melting temperature, but rather a melting temperature range, in which the fraction of melt grows as a function of temperature. The range can be several hundred degrees from the initial melting (*solidus*) temperature to the fully molten (*liquidus*) temperature. The melting behaviour of these mixtures can be illustrated using phase diagrams. [85, p. 277][125, p. 513–515]

Fully or partially molten ash particles could adhere to each other or heat transfer surfaces in the boiler. The adhesiveness of a specific ash particle is a function of the fraction of melt in it. Particles with a melt fraction between 15–70 % are considered adhesive enough to deposit on heat transfer surfaces. The temperatures, where these melt fractions are reached, depend on the composition of the ash particle. [85, p. 277–280][125, p. 513–515]

The liquid phases appearing in ash are often categorized into salt mixtures and silicates [10, p. 2824][101, p. 56][6]. However, this is a simplification, since most of the liquid phases consist of primarily ionic compounds [67, p. 130]. In this thesis, phosphates are separated as a third group.

The liquids known as salt mixtures consist of ionic compounds of metal cations and relatively simple anions. Some typical anions are Cl^-, $SO_4{}^{2-}$, $CO_3{}^{2-}$, O^{2-}, S^{2-} and $PO_4{}^{3-}$.

[67, p. 130] Molten salt mixtures typically have a low viscosity, which is roughly in the same order of magnitude as that of water (1 mPa s) [67, p. 138][101, p. 56]. The viscosity of salt mixtures does not change dramatically with composition or temperature at normal combustion temperatures. Salt mixtures are typically more volatile than silicates, and found in the fly ash. The melting temperatures of the mixture compounds are highly variable, ranging from 318 °C for $ZnCl_2$ to 2597 °C for CaO. Some waste-derived salt mixtures that contain $ZnCl_2$ and $PbCl_2$ could melt at temperatures as low as 200 °C. [67, p. 130, 134, 138]

Silicates are compounds consisting of $(SiO_4)^{4-}$-tetrahedra, which can be separate or linked to each other in different ways to form polymeric anions. Charge-balancing metal cations can also be present in many different configurations. [22, p. 107] Silicate melts often have a high viscosity and a low volatility and end up in the bottom ash [67, p. 130].

Silicates differ from salt mixtures in that they can form an *amorphous* phase upon cooling [101, p. 56]. In this case the melt does not crystallize even if temperature is lowered below the liquidus temperature of the compound. Instead, a high-viscosity melt is formed. [85, p. 281–282] For the amorphous *silicate melt*, the concept of the melt fraction determining the adhesiveness is not sufficient. The melt viscosity also needs to be taken into account [125, p. 515][67, p. 138][85, p. 282][7, p. 406]. Estimates for the maximum adhesive viscosity of silicate melts range from 10^4–10^8 Pa s [85, p. 282][113, p. 4][95, p. 277].

The relation of the viscosity of silicate melts to their temperature and composition is not completely understood. Modelling is complicated by many things, such as the fact that the silicate melt can also crystallize partially, which obviously has an effect on the viscosity. Vargas et al. [109] have summarized the effect of different metal cations on the viscosity of silicate melts.

As a base rule, the addition of metal cations to the network will always result in a decrease in viscosity. For instance, forms of silica, like quartz, represent a silicate network with no added cations [129, p. 447]. Depending on the atmosphere, quartz has a melting temperature of at least 1420 °C [19, p. 73], which is too high to cause problems in FBC. However, with introduction of potassium ions into the quartz network, the initial melting temperature of the resulting compound can be lower than 800 °C. For example, the solidus temperature of the mixture of quartz and potassium tetrasilicate $K_2Si_4O_9$ is 767 °C, according to a binary phase diagram. The lowest solidus temperature of potassium silicates is 742 °C. [13, p. 882][89, p. 242]

In a silicate melt with both alkali and alkaline earth metal cations, alkali metals typically lower the viscosity, while alkaline earth metals raise it [14, p. 88][109, p. 295]. Calcium can also force potassium out of the silicate, into the gas phase [107, p. 699]. The effect of other elements like Al and Fe is more complicated and depends on the melt composition [109, p. 295]. There is evidence in the literature indicating that Al results in an increase in the melting temperature in FBC conditions [104, p. 74–75][105, p. 5661][13, p. 890].

Phosphates are present in the molten ash of phosphorus-rich fuels. Alkali and calcium

orthophosphates melt at very high temperatures. For example, K_3PO_4 melts at a temperature between 1325–1620 °C. However, phosphates can form polymeric anions in a similar way to silicates and show some similar patterns of behaviour. These phases have lower melting temperatures, high viscosity and can form an amorphous phase when cooled. [67, p. 136] The lowest melting temperature of mixtures of KPO_3 and $K_4P_2O_7$ is about 610 °C [71, p. 4726].

As with silicates, it seems that phosphates containing higher fractions of Ca and Mg, in comparison with K or Na, melt at higher temperatures [105, p. 5661][126, p. 6383][68, p. 717]. Phosphates are also miscible with silicate melts and can reduce the melting temperatures of these phases. Additionally, many alkali salts are miscible with alkali phosphates. Lindberg et al. [67, p. 136] have compiled solidus temperatures of some K-phosphates mixed with KCl and K_2SO_4 from different literary sources.

2.3.4 Ash deposition in the boiler

Ash-related operational problems are categorized based on their location in the boiler, as shown in figure 2.4.

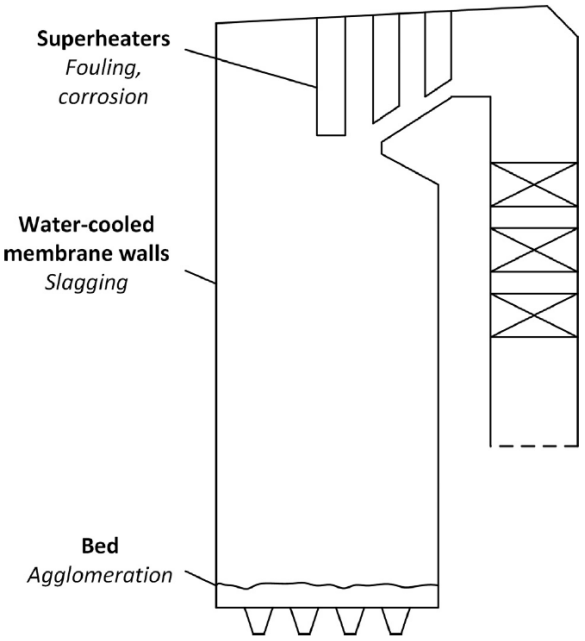

Figure 2.4. *Locations of different ash-related problems, a BFB boiler used as an example [72, p. 454].*

Ash compounds may *deposit* on colder surfaces in the boiler as solid particles, or through condensation of gaseous compounds. Deposit layers reduce heat transfer and may enhance further deposition and corrosion. Deposits forming on the radiant section of the boiler are called slag, whereas deposits in the convective pass on superheater tubes are called fouling deposits. Fouling deposits typically contain lower amounts of molten phase compared to slagging deposits exposed to the radiation heat transfer from the furnace.

[70, p. 153–155][85, p. 275–276, 284] Deposition on bed particles in the fluidized bed may result in bed agglomeration.

3 MECHANISMS OF BED AGGLOMERATION

Bed agglomeration is a complex process, in which both physical and chemical mechanisms play a role. Many different aspects of agglomeration need to be considered to obtain a full picture of the phenomenon. [12, p. 635][56, p. 3731–3732] The interdisciplinary nature of bed agglomeration, the large amount of studies and the complexity of the processes involved has led to the use of multiple different categorizations and terms for the same phenomena [56, p. 3715]. For example, the categorization of Skrifvars et al. [102], which is based on ash sintering mechanisms, has been used in some studies [81, p. 2029][56, p. 3717].

In this thesis, bed agglomeration is first discussed in terms of *melt formation* mechanisms. Next, *agglomeration* and *sintering* of wet particles is considered at the scale of individual particles. After this the bed-scale effect of *defluidization* is briefly described. These phenomena overlap with one another to a certain degree and could occur simultaneously in the bed. Finally, *chemical reaction sintering* and *molecular cramming* are discussed separately, since they differ from other mechanisms in that they do not necessarily involve fuel ash. Other agglomeration-related phenomena like build-up of electrostatic charge are not discussed in this work, since there is no evidence of them being relevant in FBC of biomass. [12, p. 638–639][72, p. 458]

3.1 Melt formation mechanisms

Agglomeration in a fluidized bed occurs when the magnitude of attractive forces between bed particles becomes comparable to the magnitude of the drag and gravitational forces keeping the particles apart [39, p. 931][97, p. 3]. Many types of *interparticle forces* may exist in the bed, and their relative importance depends on the process conditions [128, p. 3382–3384]. For example, when very fine bed particles ($<$100 µm) are used in a dry environment, *Van der Waals forces* can induce agglomeration [97, p. 3][98, p. 19][116, p. 5]. However, the general consensus among researchers seems to be that in combustion applications, agglomeration occurs through the formation of a molten phase [16, p. 832][125, p. 521][12, p. 635]. The adhesive forces caused by the presence of a melt are much larger than other interparticle forces [97, p. 3][80, p. 106][96, p. 262].

The melt developed in the bed consists of a mixture of simple salts, silicates and phosphates, as was discussed in chapter 2.3.3. The primary melt type reported in the agglomeration literature is the silicate melt. [10, p. 2824] Phosphates are observed in the

combustion of phosphorus-rich fuels [46]. Melt formation can happen through reactions between the fuel ash and bed material or entirely by ash melting [85, p. 287]. Agglomeration mechanisms corresponding to these two types of melt formation are commonly called *coating-induced* and *melt-induced agglomeration*, respectively [72, p. 454][39, p. 932][10, p. 2824][112, p. 8].

3.1.1 Coating-induced agglomeration

The most common bed material [51, p. 8][62, p. 655][119, p. 12] natural sand (also called silica sand or quartz sand), contains up to 100 wt–% of quartz [99, p. 1]. During combustion, quartz particles are covered in ash, and chemical reactions in the coating may lead to the formation of an adhesive, silicate-dominated melt. Agglomeration facilitated in this way is often called coating-induced agglomeration [72, p. 454][39, p. 932][10, p. 2824][112, p. 8]. Ash sintering -based names include *partial melting with a viscous flow* and *viscous flow sintering* [81, p. 2029][102, p. 173].

The coating is formed gradually during the combustion process, starting as individual ash deposits on the bed particle [112, p. 37]. There is some disagreement in the literature over how exactly the ash deposition happens. Figure 3.1 shows the four mechanisms proposed by researchers.

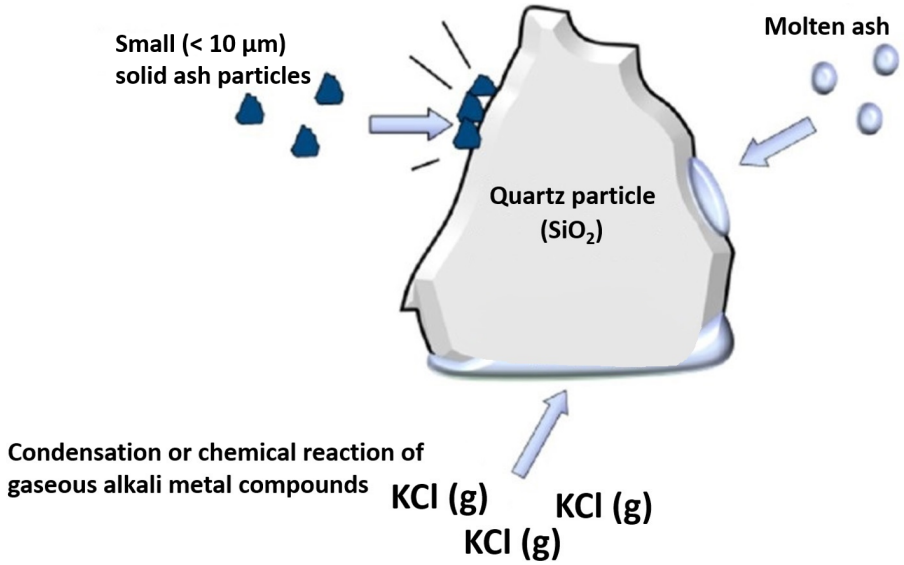

Figure 3.1. *Ash transport mechanisms, adapted from [39, p. 932].*

Ash components could end up on the bed particle either as *small (<10 µm) solid particles* [39, p. 932], *partially or fully molten particles* [39, p. 932][66, p. 179–180], or through *condensation or chemical reactions of gaseous alkali metal compounds* [77, p. 179]. Examples of gas-solid chemical reactions that could cause low melting potassium silicates to form were presented in equations 2.1–2.3.

Some researchers have ruled out condensation [93, p. 131] or chemical reactions of alkali metals as a transport pathway [39, p. 937–938]. Many studies simply consider all

the pathways as viable [16, p. 829][77, p. 179][50, p. 1672]. Some researchers have classified the chemical reactions involving gaseous alkali metal compounds as their own agglomeration mechanism, which apparently does not require coating formation [16, p. 832][30, p. 2664].

However the ash transport happens, it typically leads to a two-layered coating on the bed particles. In some cases, a third *inner-inner layer* rich in potassium has also been observed. Its presence has been attributed to high potassium content in the fuel. The final layer composition is influenced by the specific fuel used and may vary between individual particles. [77, p. 175–176][112, p. 36] One example of the composition of the two-layered coating is shown in table 3.1.

Table 3.1. *Example compositions of the two layers formed in coating-induced agglomeration [112, p. 36].*

	Inner layer	**Outer layer**
	wt–%	wt–%
Ca	41	28
Si	14	3
K	-	7
P	-	5
S	-	4

Most of the elemental composition is taken up by oxygen, which is often excluded from the tables. The *outer layer* is usually granular and its composition resembles that of the fuel ash [78, p. 1748][16, p. 832][113, p. 3–4]. According to Gatternig and Karl [39, p. 932], the outer layer is also depleted in K and Ca. The *inner layer* is more homogenous, containing Ca- and K-silicate compounds [48][46][39, p. 932]. It has the same composition and structure as the binding material in agglomerates, which implies that this layer is the cause of agglomeration [17, p. 1191][73, p. 132][81, p. 2034]. Scanning electron microscopy (SEM) analyses indicate that the inner layer has an amorphous structure and that it was in a molten state during combustion. Gatternig and Karl have suggested that the outer particle layer is floating on the surface of the inner molten layer. [39, p. 932, 937]

The thickness of the coating is typically in the range of 1–70 µm [73, p. 131][113, p. 2] and increases with longer retention times in the furnace [48, p. 3843]. Visser et al. [113, p. 2][114] have reported 1.5 µm as a minimum critical thickness for defluidization to occur. Brus et al. [18, p. 10] also found the critical thickness to be less than 10 µm.

Building on previous work of other researchers [123, p. 824][16], He et al. [48] have proposed a three-stage mechanism for coating formation, shown in figure 3.2. Durations for each stage were obtained by studying samples from a 30 MW_{th} BFB boiler that used a wood-based fuel mixture with 1.8 ± 0.51 wt–% ash, 0.12 wt–% Si, 0.44 wt–% Ca and 0.11 wt–% K out of dry matter. [48, p. 3842–3847]

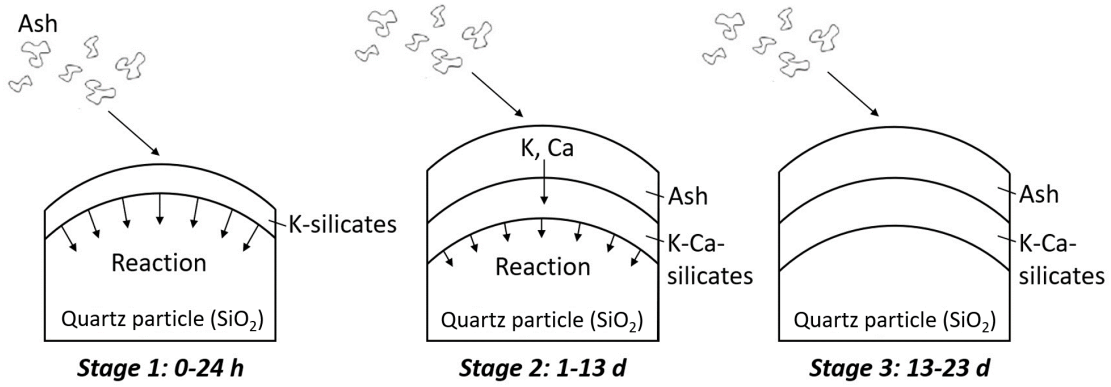

Figure 3.2. *Stages of coating formation, edited from [72, p. 459]. Layer thicknesses are not to scale.*

In the first stage, a thin and homogenous melt layer forms on the bed particle. The layer mainly contains potassium, which reacts with quartz on the bed particle surface, lowering the solidus temperature of the system. The absence of an outer particle layer can be explained by fast reactions between incoming ash particles and quartz. [125, p. 523][48, p. 3846–3847]

The adhesive melt enables coarse ash particles with CaO and MgO to attach to the bed particle. Ca^{2+} and Mg^{2+}-ions could subsequently start to dissolve into the melt, shifting the silicate composition to areas with higher melting temperatures by forming compounds like $CaSiO_3$. Mg seems to be less reactive than Ca, mostly staying in the outer layer. [48, p. 3846–3847] The increasing proportion of alkaline earth metals in the melt could also lead to release of alkali metals to the gas phase [107, p. 699].

In the second stage, the growing amount of Ca and Mg compounds in the melt has decreased the K/Ca ratio and the fraction of melt in the inner layer dramatically. A particle-rich outer layer forms, indicating slower reactions compared to the rate of ash accumulation. In this way the particle coating grows outward through ash matter transport, and inward through reactions in the bed particle. The inner layer growth rate is high at first, but decreases over time. He et al. explain this by the lower rate of diffusion resulting from the increasing thickness and decreasing melt fraction of the inner layer. [48, p. 3846–3847]

During the last stage of coating formation, the calcium silicate layer prevents further diffusion of potassium to the bed particle interface, leading to a reduced agglomeration tendency. More complex calcium silicates like Ca_2SiO_4 and Ca_3SiO_5 continue to form in the inner layer. Because of the low melt fraction in the inner layer, the reactions with calcium and consequentially also the layer formation rate are controlled by solid-state diffusion, which is relatively slow. [48, p. 3846–3847] The presence of a protective calcium layer has also been observed by many other researchers [11, p. 261][62, p. 659][34, p. 707][82, p. 345].

He et al. noted that in the samples from CFB combustion, the outer layer was much thinner compared to those from the BFB boiler. This could be because of the more

severe attrition experienced by particles in a CFB. As a result, there might be less calcium available to diffuse into the inner layer and lower the amount of melt. This could explain why CFB samples had a higher K/Ca ratio in the inner layer. [48, p. 3846]

Even if the adhesiveness of the coating is reduced in the final stage of coating formation, there are other ways how agglomeration can proceed for coated particles, as shown in figure 3.3 [50, p. 1676].

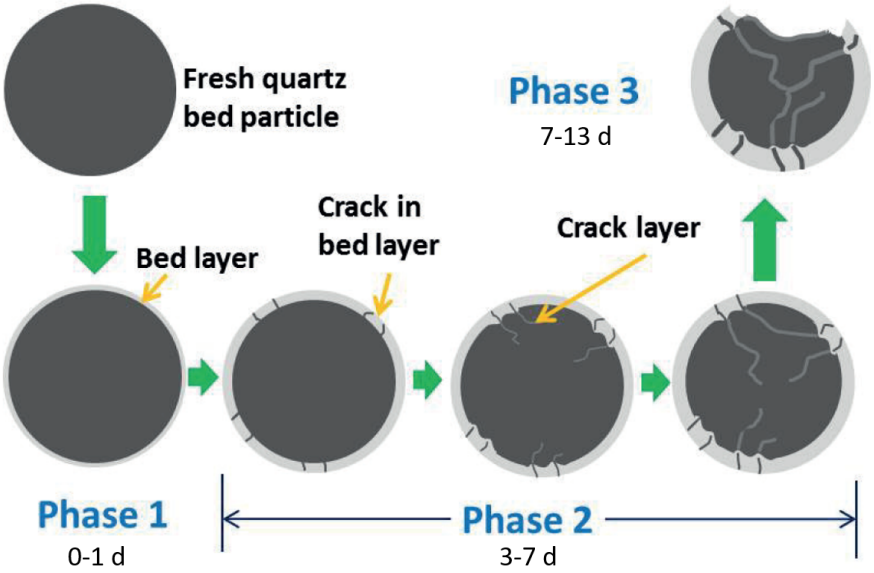

Figure 3.3. *The phases of crack layer formation [50, p. 1676]. Phase durations were determined from the same samples as the durations of the stages of coating formation in figure 3.2.*

After the initial layer formation, fractures may appear in the inner coating layer, and the resulting tension can cause cracks to form in the bed particle itself. Gas-phase K compounds are then able to diffuse along the connected fractures in the inner layer and bed particle. They react with the bed material, accompanied with a small amount of Ca, forming an alkali silicate -dominated layer in the fracture. Additional K may diffuse further into the fracture, propagating the reaction inwards. *The crack layer* propagation continues and the fractures widen and connect with each other. Widened fractures enhance K diffusion towards the core of the particle and increase melt formation. Subsequently, a large portion of the bed particle is transformed into an alkali silicate melt and sticky fragments might separate from the particle, exposing the molten crack layer. Both the fragments and the exposed layer could facilitate agglomeration. This mechanism could also explain the occasional presence of an additional K-rich inner-inner layer in the coating. [50, p. 1673, 1676]

3.1.2 Melt-induced agglomeration

In some cases the fuel ash by itself contains the necessary components for the formation of the adhesive molten phase. Agglomeration facilitated in this way has been called

melt-induced agglomeration [112, p. 8][115, p. 2], liquid-induced agglomeration [39, p. 932][43], partial melting [81, p. 2029][102, p. 173] and reactive liquid sintering [102]. All the names are somewhat misleading, since the formation of melt is a crucial factor in agglomeration also in the coating-induced mechanism [56, p. 3715–3716]. Some sources seem to have defined partial melting to be the term describing melt-induced agglomeration caused specifically by salt melts [81, p. 2029][102, p. 175].

A typical characteristic of melt-induced agglomeration is the absence of fully coated bed particles. Only small areas of the particle surfaces are wetted by the adhesive melt. The composition of the particle bonds resembles the global ash composition. [56, p. 3716][39, p. 932, 938–939][69, p. 6512][112, p. 8] Figure 3.4 shows the two sub-mechanisms associated with melt-induced agglomeration.

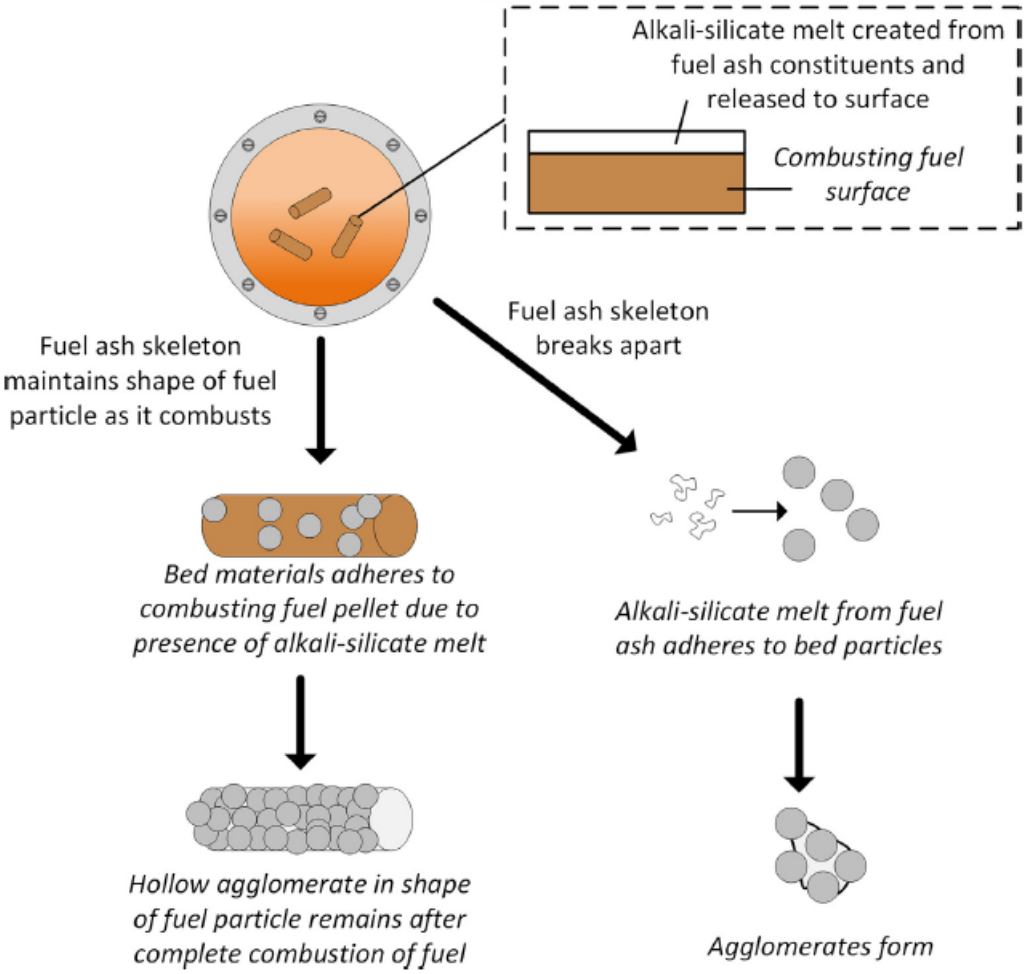

Figure 3.4. *The two sub-mechanisms of melt-induced agglomeration [72, p. 460].*

The more straight-forward one is shown on the right, where molten ash detached from burning fuel acts as a glue between bed particles [112, p. 8]. The mechanism was first discovered by Gluckman et al. [43] and has subsequently been recognized by many other researchers [39, p. 931][16, p. 831][29, p. 5324][81, p. 2036][69, p. 6512]. The left hand side of figure 3.4 shows an alternative mechanism, which was first suggested by Lin et al. [66, p. 179]. If the fuel particle maintains its shape while combusting, the bed particles

could adhere to the ash melt formed on its surface, becoming submerged in it. When combustion is finished, the bed particles remain stuck together, and an agglomerate in the shape of the fuel particle remains. This mechanism has also been later observed by other researchers [26, p. 78–79][93, p. 128][25, p. 743].

3.2 Particle-scale agglomeration and sintering

In addition to the larger-scale phenomena mainly focused on melt-formation, agglomeration has also been studied in the smaller scale. When a liquid phase forms to the fluidized bed as a result of the mechanisms described above, it can be assumed that the dominant interparticle forces arise from *liquid bridges* and *sintering* [96]. In general, the researchers assumes *viscous flow sintering* as the binding mechanism between agglomerated particles without further discussion or physical justification [10, p. 2826]. However, according to several research groups [56, p. 3716][37, p. 3–4][97, p. 3], the initial particle-scale agglomeration in the fluidized bed happens through liquid bridges, while sintering may act to strengthen the agglomerate bonds. These views are not necessarily mutually exclusive, if viscous flow sintering is the mechanism responsible for strength development in agglomerates. In any case, both phenomena are discussed in this section.

3.2.1 Liquid bridges

A liquid bridge may form between bed particles, if a collision happens in a wet region of either or both of the particle surfaces [56, p. 3728]. The interparticle forces related to liquid bridges consist of the static *capillary force* and the dynamic *viscous force* [28, p. 1868].

The capillary force arises from the combined effect of surface tension and the pressure deficit within the liquid bridge. The magnitude of this force is determined by the surface tension of the liquid, bridge volume and the separation distance between particles. In a fluidized bed, the wet particle surfaces are not stationary, but constantly moving relative to each other. This introduces a dynamic dissipative force, the magnitude of which depends on the viscosity of the liquid and the relative particle motion. [83, p. 27][97, p. 4][28, p. 1868] Figure 3.5 shows the formation of a liquid bridge during a collision between identical uniformly coated wet particles, along with the forces involved.

Collision models often divide the process into three stages [97, p. 6][8, p. 4048–4049][28]. In *the approach stage* the liquid is squeezed between the particles. The kinetic energy of the particles increases due to the capillary force $\mathbf{F_c}$ and decreases as a result of the viscous dissipation force $\mathbf{F_d}$. In *the solid-solid contact stage* the particles experience an inelastic collision and some of their kinetic energy is again dissipated. In *the separation stage*, the particles rebound and both the capillary and viscous forces result in a decrease in their kinetic energy. Agglomeration can occur if the kinetic energy of the particles is completely dissipated during either the approach or separation stage. [97, p. 6][28] The

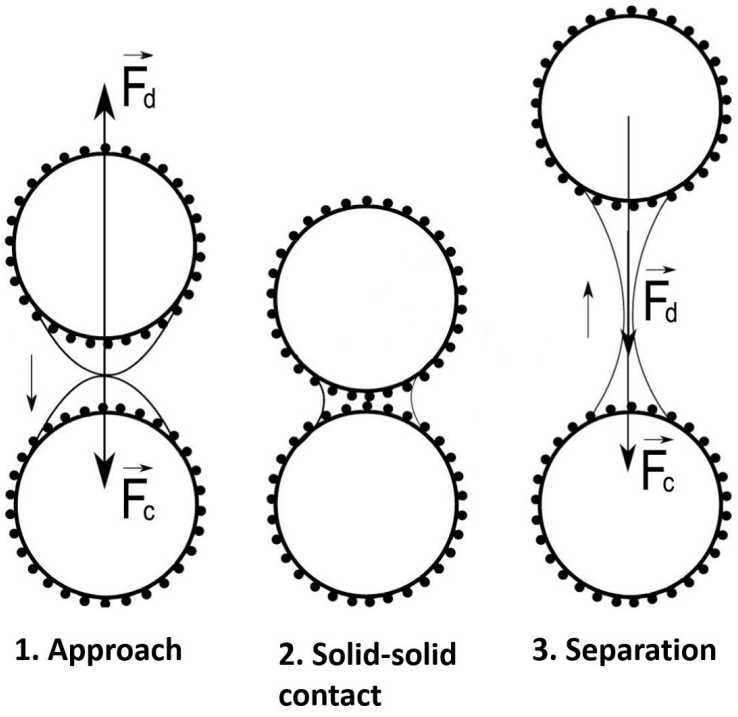

Figure 3.5. *A collision between identical coated wet particles, adapted from [9, p. 592].*

newly formed agglomerate could still break if the bond is not sufficiently strong to withstand the hydrodynamic forces in the bed. However, according to Balland et al., once a liquid bridge is formed, it will rarely break under fluidization. [10, p. 2838]

The relative magnitude of the capillary and viscous forces can be assessed based on a dimensionless capillary number $\mathbf{Ca} = \mu \cdot \mathbf{v_{rel}}/\gamma$, where μ is the viscosity of the liquid, $\mathbf{v_{rel}}$ is the relative velocity between particles and γ is the surface tension. The viscous force dominates if the value of $\mathbf{Ca}$ is greater than 1, whereas the capillary force is prevalent when $\mathbf{Ca}$ is less than 10^{-3}. The parameter with the most variation out of the three is usually viscosity, and therefore its variation governs the value of $\mathbf{Ca}$. [97, p. 4] In FBC, high-viscosity liquids, such as silicates are often encountered and for them the viscous dissipation forces dominate agglomeration [56, p. 3716].

This is a simplified model to illustrate the adhesion of two liquid-coated particles during collisions. In the real FBC process, the particles are not spherical and could consist of different materials and have different surface properties. The liquid layers can be dispersed on the particles differently and have non-identical compositions. [97, p. 6] Liquid bridges could also form simultaneously between multiple particles, if a sufficient amount of liquid is present. More research is still needed in order to understand the behaviour of these kinds of bonds. [15, p. 26–27]

3.2.2 Sintering

In other industries, such as ceramics and powder metallurgy, sintering is an important processing technique, which is used to transform powders into larger solid bodies [22, p. 438]. In agglomeration research the term *sintering* is used quite freely [125, p. 520][99, p. 2] and sometimes as a synonym for agglomeration [81, p. 2028]. In this thesis, sintering is treated as one of the physical phenomena involved in bed agglomeration.

Seville et al. [96, p. 264] define sintering as a mass transfer process, where material migrates to the area of contact to form a neck. Sintering is driven by minimization of *surface energy*. The atoms or molecules on the surface of a particle possess higher energy than those closer to the center. The system strives for lower energy by reducing the surface area. Smaller particle sizes and higher temperatures typically accelerate the process. [96, p. 265][84, p. 33][91, p. 66][88, p. 218–223] Figure 3.6 illustrates the sintering of two spherical particles. The dashed lines show the original particle boundaries.

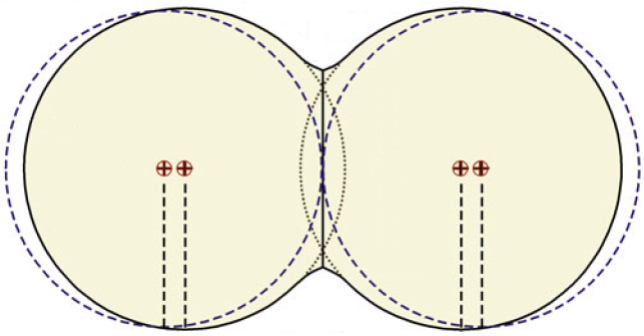

Figure 3.6. *Sintering of two spherical particles, edited from [22, p. 442].*

Sintering mechanisms can be categorized based on the mass transfer mechanisms involved. *Solid-state sintering* refers to the sintering of a polycrystalline solid, single-phase particles in a temperature, which is lower than their melting temperature. Matter transport in solid-state sintering may happen by at least six different mechanisms that can operate simultaneously. [84, p. 32–35, 470–471] According to Khadilkar et al. [56, p. 3716], solid-state sintering is too slow to be the main cause of bed agglomeration in FBC.

Liquid-phase sintering refers to sintering in the presence of a small amount of additive, which forms a liquid phase between the particles. The liquid phase can also be formed through melting of the additive or a reaction between the additive and the main component. The liquid phase enhances the diffusion of material between particles, assisting in sintering. A special case of liquid-phase sintering is *viscous flow sintering* (or *viscous sintering*, *vitrification*), in which the liquid is highly viscous and forms a glassy phase upon cooling below the solidus temperature. In this case the mass transfer occurs through slow viscous flow under the action of capillary forces. Viscous flow sintering is the main sintering mechanism in systems that consist of silicates. [84, p. 33–35, 622–623, 678][85, p. 282]

For a group of adjacent particles, the progress of sintering is shown in figure 3.7. Sintering

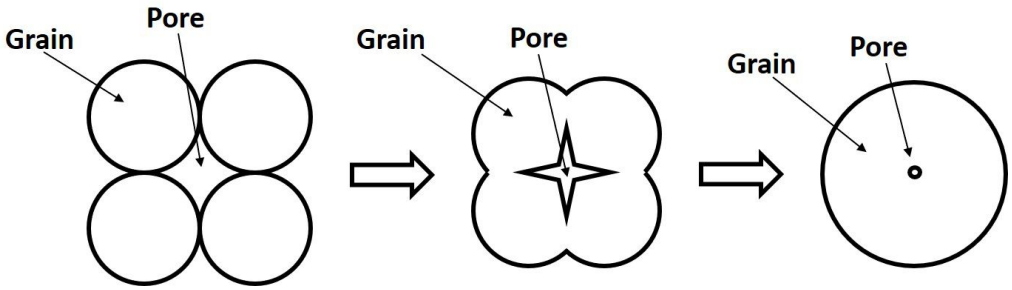

Figure 3.7. *Sintering of a group of spherical particles, adapted from [21, p. 524].*

begins by formation of necks between particles. Eventually, the connected particles form a porous network. As the process continues, the pores start to close so, that individual particles can no longer be recognized. The result is a continuous, dense material with strong bonds between particles. [101, p. 55][102, p. 171][88, p. 217]

3.3 Progress of defluidization

Agglomeration probably begins in the high-temperature locations of the fluidized bed and around particles that contain material more susceptible to melting than the average bulk [55, p. 182]. As the amount of liquid on the particles increases, Geldart group B particles can change their behaviour through group A to group C, and become difficult to fluidize. The first agglomerates disturb mixing and bubble formation, which leads to an increase in temperature peaks and quiescent regions in the bed. These changes could then further promote agglomeration. [10, p. 2838][12, p. 636]

Agglomerates will gradually segregate at the bottom of the bed, once they are too heavy to be held afloat by the fluidization air [10, p. 2832]. Figure 3.8 shows the progress of this segregation in a lab-scale fluidized bed.

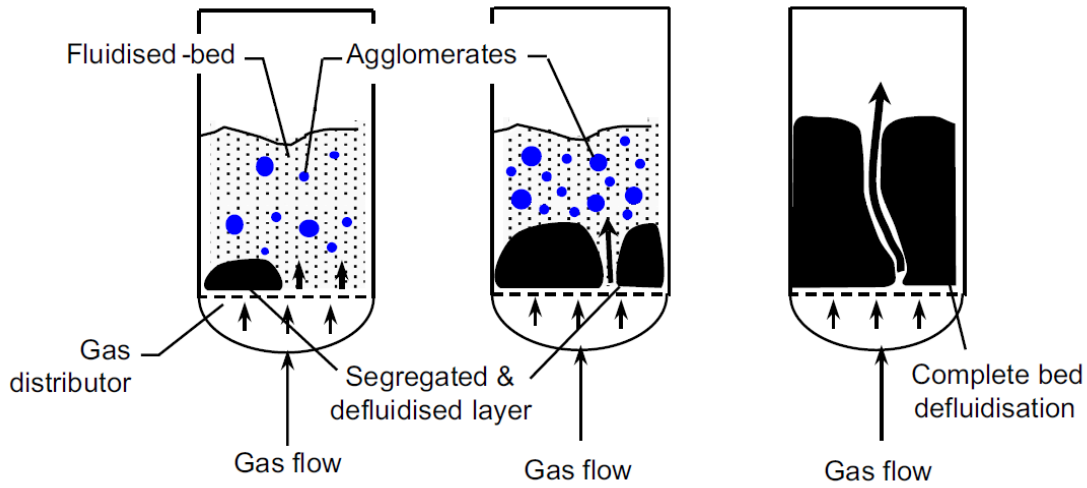

Figure 3.8. *Progress of agglomeration, edited from [10, p. 2835].*

The segregated layer grows over time and once it obstructs most of the gas distributor

section, fluidization air starts to flow through preferential channels in the layer. This leads to non-uniform air distribution, and finally, to the full defluidization of the bed. [10, p. 2832] In this case the group of particles no longer resembles a fluid and the bed collapses to a fixed bed, causing a sharp decrease in the pressure drop and significant temperature changes [39, p. 931][125, p. 520–521]. If the temperature remains high enough, the lack of particle movement in the fixed bed leads to even more severe agglomeration and sintering [56, p. 3716].

3.4 Chemical reaction sintering and molecular cramming

Chemical reaction sintering (or *reaction-induced sintering* [125, p. 509][51, p. 8]) is a phenomenon, in which binding material is formed between contacting particles through chemical reactions with gas-phase compounds [102, p. 174][4, p. 1933]. The term is usually used in the context of CFB boilers, when limestone addition is used to control sulfur emissions. Lime particles may react with sulfur oxides in sulfation reactions (eq. 2.6) or with carbon dioxide in recarbonation reactions (eq. 2.7), forming a dense solid material, which binds particles together [51, p. 8][102, p. 174–175]. Chemical reaction sintering is typically associated with deposit formation and strength development, for instance in the cyclone of a CFB boiler. Agglomeration of bed material by this mechanism is reported in the return leg of CFB boilers, and not in the fluidized region. [100, p. 215][125, p. 509]

Anthony et al. [4, p. 1933] link chemical reaction sintering to another phenomenon called *molecular cramming*. In molecular cramming, chemical reactions increase the molar volume of a compound, causing it to fill the pores in a confined mass of material. Sulfation of calcium (eq. 2.6) is expected to be the main reaction at fault. Molecular cramming is relevant for deposition when high amounts of S and CaO are present and could take place in the return leg of CFB boilers. It is questionable whether it has any significance for the fluidized bed, where the particle separation forces are larger, no volumetric restrictions are present and particles are removed continuously. [12, p. 638–639][3, p. 58]

4 EFFECT OF OPERATIONAL PARAMETERS ON BED AGGLOMERATION

On the particle level, bed agglomeration requires three things: that the bed particles collide, the collisions occur in the melt-covered areas of the particle surfaces and that the melt properties are suitable to glue the particles together [56, p. 3728].

The frequency of bed particle collisions depends on the hydrodynamic properties of the bed, such as void fraction and fluidizing gas velocity. The probability of a single collision being wet depends on the extent of melt coverage on the particles, which in turn depends on bed hydrodynamics, gas atmosphere as well as the amount and characteristics of the melt and bed material. The amount and properties of the melt are determined by the fuel composition, or both the fuel and bed material composition, depending on the dominant agglomeration mechanism. [56, p. 3724, 3726–3727]

A further complication in these relationships is introduced by the fact that the values of the relevant parameters may vary locally and temporally during agglomeration. For example, agglomeration increases the average bed particle size, which leads to decrease in void fraction and particle velocity. [56, p. 3726] The description of all the parameters and their coupled effects is out of the scope of this thesis. Instead, some of the most important ones are discussed. More comprehensive reviews can be found from Khadilkar et al. [56] and Morris et al. [72, p. 460–469].

4.1 Temperature

Extensive research [66, p. 175][92, p. 255, 264][122, p. 4540][24, p. 2920] has confirmed that increasing the bed temperature leads to faster agglomeration and defluidization as a result of many factors. First of all, a higher temperature results in a larger amount of melt in the bed. Additionally, temperature controls the viscosity of the molten phase. [66, p. 175][39, p. 939] According to a diffusion model by He et al., there is also a significant increase in the growth rate of bed particle coatings at higher temperatures [49, p. 2230]. This would mean that the critical layer thickness in coating-induced agglomeration is reached faster. Finally, the rate of mass transfer in different sintering mechanisms is also a function of temperature [88, p. 221–223][96, p. 265].

Even though temperature has such an evident effect on agglomeration severity, bed temperatures are usually constrained by steam requirements of the boiler, and cannot be

altered solely based on bed conditions [72, p. 461][12, p. 656]. Another important fact about temperature is that it is not completely uniform throughout the fluidized bed, but varies locally, enabling agglomerates to form even at lower average bed temperatures. In biomass combustion, a significant amount of fine carbon particles is generated and they might experience peak surface temperatures exceeding the bed temperature [27, p. 2282][94, p. 239], possibly to the extent of 40–600 °C [74, p. 10].

4.2 Fluidizing gas velocity

Several researchers have looked into the effect of fluidizing gas velocity on agglomeration. Fluidizing gas velocity can be normalized between different bed materials by using *the fluidization number*, which is the ratio of fluidizing gas velocity $\mathbf{U}$ to the minimum fluidization velocity $\mathbf{U_{mf}}$ of the material [39, p. 934]. Fluidizing gas velocity can be increased without changing the combustion conditions through the use of nitrogen.

It seems clear that increasing $\mathbf{U}$ or $\mathbf{U/U_{mf}}$ will reduce the rate of agglomeration. [66, p. 175–176] For example, in the experiments of Gatternig and Karl [35, p. 164], who used coffee skins as fuel and 800 °C as bed temperature, an increase of $\mathbf{U/U_{mf}}$ from 8 to 12 prolonged the time until defluidization by at least 72 h. The increase in momentum decreases the likelihood of particles adhering to each other and molten ash. Mixing is also enhanced, which leads to fewer areas with poor fluidization. [66, p. 176] However, increasing the fluidizing gas flow could be just a temporary strategy, since it does not counteract melt formation in the bed. Furthermore, as with bed temperature, raising the gas velocity has a drastic effect on the boiler process and can be considered an emergency measure. [12, p. 656]

4.3 Fuel

The composition of ash-forming matter in the fuel is one of the most crucial parameters influencing bed agglomeration [40, p. 11]. The main elements affecting agglomeration tendency seem to be K, Ca, Si and P. Additionally, the chemical behaviour of Na and Mg is similar to K and Ca, respectively. In general, the severity of agglomeration increases with increasing alkali metal content. If the fuel also contains enough inherent reactive Si, it is predisposed to melt-induced agglomeration. Herbaceous fuels like straw are typically associated with this category. [16, p. 831][72, p. 462] Fuels with relatively high amounts Ca typically have a lower agglomeration tendency. These include most wood-derived fuels and they will predominantly follow the coating-induced mechanism. [46, p. 937]

For phosphorus-rich fuels, ash transformation reactions are governed by phosphorus, due to the higher stability of most phosphate compounds. The basic oxides of K, Ca and Mg are converted into phosphates, which reduces the amount of K able to react with bed material, preventing coating formation. However, the partially molten ash particles rich in phosphate could adhere and react with the bed material and form discontinuous sili-

cate/phosphate layers that induce agglomeration. [46, p. 946][13, p. 890] No quantitative definition was found of how much phosphorus is necessary for a fuel to be phosphorus-rich. Based on studies using the term "*phosphorus-rich*" [68, p. 711][81, p. 2032][46, p. 939][117, p. 547], the element is at least considered prevelant when it constitutes more than 0.40 wt–% of the dry matter of the fuel, or 27 wt–% on ash oxide basis.

Quantitative estimates for ash element compositions that result in a certain type of agglomeration are scarce in the literature. Piotrowska et al. [81, p. 2035] conducted combustion experiments in a bench-scale BFB reactor with different ratios of rapeseed cake and bark. They used coating thickness measurements to infer the dominant agglomeration mechanism for each fuel blend. They concluded that for mixtures with between 0–40 wt–% bark the dominant mechanism was melt-induced agglomeration. For mixtures with over 60 wt–% bark the coating-induced mechanism was the primary one. This corresponded to a Ca/P ratio larger than 1.27 and a (Na + K)/(Ca + Mg) ratio lower than 0.8. For the mixture with 50 wt–% bark it was not possible to determine, which mechanism was dominant.

In addition to composition, fuel density might also affect agglomeration. Low-density fuels like straw are not properly submerged in the bed in BFB boilers and only float on its surface. This reduces heat transfer from the burning fuel, resulting in excess temperatures that promote agglomeration. [39, p. 939]

Combustion of fuels with high agglomeration tendency can be achieved through the use of fuel *co-combustion* or *pre-treatment*. Co-combustion reduces the relative amount of the problematic fuel. The technique has mainly been used with coal–biomass- and wood–straw-mixtures. One example of fuel pre-treatment is leaching with water, which has successfully prevented agglomeration for some fuels. [12, p. 656][72, p. 462–468]

4.4 Bed material

In coating-induced agglomeration the adhesive molten phase forms in chemical reactions between compounds in the fuel ash and quartz in the bed material. Therefore, it is logical to study the use of *alternative bed materials* that do not contain quartz as a way to prevent agglomeration. [72, p. 465][12, p. 660–661]

A large amount of different bed materials has been tested, summary of which can be found from Bartels et al. [12, p. 659–661] and Morris et al. [72, p. 464]. Examples include *olivine*, *blast furnace slag*, *diabase*, *bauxite* and *ilmenite*. Alternative bed materials usually comprise of aluminium, magnesium, calcium, iron and their compounds. Materials including these elements have been shown to reduce agglomeration tendency. [12, p. 660–661] Mixing of different bed materials could also be a cost-effective option in some cases [62]. It has also been noted that using quartz-free bed materials might not be sufficient to prevent agglomeration in all circumstances. Fuels with enough reactive Si could still form agglomerates through the melt-induced pathway. [12, p. 661][45, p. 4558][122, p. 4537–4539][30, p. 2666]

Due to the comparatively high cost and lower availability of alternative bed materials, natural sand is still usually used in the industry, even with high alkali fuels. In these cases the most common agglomeration counteraction method is the continuous replacement of used bed material [2, p. 2, 9][64, p. 143][62, p. 655–656][29]. This technique could be combined with an automatic sieving system, which removes particles over a specific size limit [12, p. 655][63, p. 50]. However, no reports were found of these methods preventing agglomeration for the most challenging fuels.

4.5 Additives

The purpose of bed *additives* is to prevent the formation of sticky molten material by diluting the problematic species, capturing condensable vapours or inducing the formation of other compounds with higher melting temperatures. Additives can be introduced to the furnace by blending or mixing them with the fuel prior to combustion, or by a separately installed spraying system. [12, p. 662][118, p. 23]

There is a large amount of different additives that have been shown to reduce agglomeration. Researchers have used magnesium and aluminium silicates, sulfur-, calcium- and phosphorus-based additives as well as carbonates and oxides of calcium, magnesium and barium. [118, p. 24][12, p. 658] One common example is *kaolin*, which has been succesfully used up to the industrial boiler scale [72, p. 467][10, p. 2832–2833]. Calcium addition has proven effective with high-phosphorus fuels [68, p. 717][11, p. 262]. A more comprehensive compilation of different additives can be found in sources by Wang et al. and Bartels et al. [118, p. 26][12, p. 656–659]. As with the use of alternative bed materials, agglomeration could still proceed if the fuel is susceptible to the melt-induced mechanism, but additives still seem to have a positive effect [72, p. 467].

5 MONITORING AND PREDICTION OF BED AGGLOMERATION

Ever since the discovery of the phenomenon of bed agglomeration, researchers have tried to find methods for predicting its occurence [35, p. 157]. The methods can be subdivided into two groups: *pre-combustion prediction* methods are employed before combustion in a full-scale facility, whereas *in-situ monitoring and prediction methods* are used during the operation of the unit [72, p. 469]. The number of different methods is large, and this chapter provides only a brief summary. More comprehensive works are available by Bartels et al. [12, p. 639–655] and Morris et al. [72, p. 469–470].

5.1 Pre-combustion prediction

The pre-combustion methods for agglomeration prediction include *fuel ash measurements*, *empirical* and *semi-empirical* modelling, as well as *lab- and pilot-scale trials*. These methods are most commonly used to predict either the minimum fluidization velocity required to avoid agglomeration, *defluidization time* or *agglomeration temperature*. Defluidization time is the time from the beginning of the combustion process until the bed collapse. Currently the most reliable methods of predicting agglomeration behaviour for a given fuel seem to be lab- and pilot-scale trials. [40, p. 2][72, p. 469]

5.1.1 Fuel ash measurements

There have been several attempts to make use of standardised fuel ash testing methods to predict agglomeration temperature. These procedures include various heating tests measuring thermal contraction or expansion, structural changes or compression strength. Their problems are mostly related to the fact that they do not take into account the reactions and fuel–bed particle interactions in the actual fluidized bed process. Fuel ash test methods seem to be reliable for a narrow range of fuels with constant properties, but in practise fuel flexibility is one of the strengths of FBC, so variation is common. [12, p. 639–642][36, p. 34–38]

5.1.2 Empirical models

Several empirical indices have been developed to predict ash-related problems based on ash component ratios. In coal combustion, these indices have been useful in predicting ash-related issues, due to the more homogenous ash compositions and larger knowledge base compared to biomass fuels. [36, p. 56] Some researchers have tried to apply these indices to predict agglomeration in biomass combustion, while others have developed entirely new ones specific to biomass [72, p. 469].

Similarly to the fuel ash measurement methods, these indices are mainly used to predict slagging or deposition. They only represent the behaviour of ash, without accounting for process parameters or reactions in the fluidized bed. Composition-based indices are therefore not very applicable in agglomeration prediction, or at least require more refining across different fuels, conditions and scales to be useful in practise. [36, p. 57][110, p. 181][72, p. 470]

Gatternig and Karl [35, p. 160] have compiled empirical agglomeration models that account for both fuel- and process-related parameters. These equations usually attempt to predict either the minimum fluidization velocity required to avoid agglomeration or defluidization time. All of the models listed showed a deviation of at least $\pm 20\,\%$ from experimental values. For their own model, which uses non-linear regression and ensemble methods to predict the defluidization temperature from a set of fuel and operational parameters, Gatternig and Karl report a predictive error of about 60 K, or $\pm 10\,\%$ [35, p. 161, 165][37, p. 2].

5.1.3 Semi-empirical models

Semi-empirical methods use some theoretical assumptions in addition to the values obtained from experiments. Certain semi-empirical models can be used to predict the chemical composition of the adhesive melt, bed hydrodynamics and agglomerate growth kinetics [36, p. 46–48, 54–55][56, p. 3718–3722]. The composition of the molten phase in the bed can be determined by simulating phase changes and chemical reactions using *thermochemical equilibrium calculations*. The process involves defining the expression of *the Gibbs free energy* for all the included chemical compounds. Next, the expression for the Gibbs free energy of the system is acquired as a weighted sum of the Gibbs energies of the compounds. Dedicated algorithms can then be employed to solve the equations for the resultant compounds and phases by minimizing the value of this sum. Because of the large number of equations, the calculations are usually performed using dedicated software, such as *FactSage*. Additional models in the program can be used to determine the viscosity and surface tension of the melt based on the obtained composition. [67, p. 130–131][38, p. 118–119, 121–122]

The results from thermochemical equilibrium calculations can be incorporated into other models. Balland et al. [10, p. 2839] presented a simple model for gasification systems,

in which defluidization time is calculated based on minimum fluidization velocity and the volumetric fraction of molten ash in the bed. Thermodynamic equilibrium calculations are required to obtain the liquid fraction in ash at the operating temperature. The model performed well in comparison with the experimental values from the same study, but the authors note that more validation should be done in future works.

The main problem with thermochemical equilibrium calculations is the lack of experimental data available for some compositional ranges of ashes. This may result in physically improbable melt formation in some cases. Also, some understanding of the different forms of ash material in the fuel is required, since only the reactive compounds should be included in the calculations [51, p. 8]. Additionally, the calculations do not take into account reaction kinetics, physical phenomena or local conditions in the bed. [38, p. 126][67, p. 139][34, p. 702]

The behaviour of a fluidized bed can be simulated using *computational fluid dynamics (CFD)*. CFD models for the simulation of gas-solids multiphase flows include *Eulerian–Eulerian* and *Eulerian–Lagrangian* methods. In the Eulerian–Eulerian approach the solid and fluid phases are both considered continuous. The main Eulerian–Eulerian method is the Eulerian–Eulerian method for granular flows. It uses the kinetic theory of granular flow to describe particle–particle interaction. [5, p. 680–681]

The Eulerian–Lagrangian methods treat the fluid phase as a continuum and the solids as a discrete phase. These models track a large number of particles in the flow field. One example of an Eulerian–Lagrangian approach for agglomeration prediction is the *CFD-discrete element method (CFD-DEM)*, in which a soft sphere model is used to track particle–particle interaction. Liquid bridge forces must be included into the force balance equation of each particle. Eulerian–Lagrangian models can be used to model particle-level interaction more accurately than Eulerian–Eulerian models, but they often have a high computational cost. Some models combining the two approaches also exist, like the *dense discrete phase model (DDPM)*, which uses Lagrangian treatment for particles in low solids volume fractions, and Eulerian treatment for particles in high solids volume fractions. [5, p. 681–683][56, p. 3721–3722][37, p. 2]

In agglomeration modelling an additional complexity arises from the change of particle size in the fluidized bed. Techniques such as *population balance models* and *Monte Carlo methods* could be used to determine the rate of agglomerate growth. Population balance models apply conservation equations to estimate the number of particles in different size intervals in a system with particle addition or removal, coating, agglomeration and breakage. This approach has not been adapted to ash-induced agglomeration and it could be challenging due to the empirical parameters required. Monte Carlo methods rely on statistical random sampling and probability. They can be integrated with population balance models or used independently. [57, p. 220][56, p. 3720–3721][37, p. 2]

Different combinations of the above models could be used to yield a comprehensive

model for agglomeration prediction. Khadilkar et al. [56, p. 3731] have proposed an algorithm for the development of an integrated agglomeration model. Gatternig and Karl [37] developed a method combining thermochemical calculations with the CFD-DEM model to determine the agglomeration temperature for a given fuel. The model is restricted to coating-induced agglomeration and not yet ready for practical use.

5.1.4 Lab- and pilot-scale trials

Small-scale experiments have generally been successful in predicting the onset of agglomeration in full-scale boilers. In the long term however, replacement of bed material and longer residence times in full-scale boilers create divergence in the coating properties in the samples. The main disadvantage of lab- and pilot-scale trials is the high cost of material and time required. [72, p. 468–470][38, p. 117]

Lab-scale trials are typically conducted in fluidized bed reactors of around 100 mm bed diameter. Stable and controllable bed temperatures can be achieved by electrical heating or gas burners. Gatternig and Karl [40, p. 2–3] have combined reactor data from different studies.

Three main experimental procedures have been used by researchers to compare the agglomeration tendency of fuels. The first is *the off-line analysis method*, in which each case is combusted for a fixed period of time. The agglomeration extent of the resulting bed is categorized to discrete classes based on visual observation, sieving or SEM analyses [79, p. 2890]. The visual classification is somewhat subjective, influencing the reproducibility and applicability of the results [40, p. 2].

The second method uses defluidization time as the indicator for agglomeration severity. As in the off-line analysis method, replacement of bed material occurring in full-scale boilers is not accounted for. Comparison of tests with varying operational parameters provides information about safe conditions for a given fuel. [40, p. 2] The defluidization time method has been relatively popular among researchers [26][69, p. 6508][106][25, p. 740].

The third method is called *controlled fluidized bed agglomeration (CFBA)* and developed by Öhman and Nordin [75]. In this two-stage method, agglomeration tendency is quantified by agglomeration temperature. First, fuel is combusted at a temperature low enough to prevent agglomeration. The process is terminated after a sufficient amount of ash has been generated. In the second stage, the ash is fed into a fluidized bed, which is gradually heated with electrical wall heating elements until agglomeration is registered. To maintain a combustion atmosphere in the furnace, propane is burned in a chamber preceding the air distributor. [75, p. 92] The resulting agglomeration temperature gives an estimation for the upper operational limit for combustion with a given fuel [40, p. 2].

The goal of the CFBA method is to eliminate the uncertainties associated with elevated temperatures near burning particles. This way different fuel- bed material combinations

can be compared more reliably. Öhman and Nordin [75, p. 91] reported precision of $\pm 30\,^{\circ}C$ and reproducibility of $\pm 5\,^{\circ}C$ for the agglomeration temperature obtained with this method and it has been used in a wide range of studies [76, p. 619][81][30][46]. The electrical heating stage has also been used to study artificially coated bed material and samples from full-scale boilers [113, p. 1–2][29, p. 5317].

Another supposed benefit of the CFBA method is the constant amount of ash in the bed, which is meant to simulate the balance of ash addition and removal in a full-scale boiler [40, p. 2]. However, some researchers have also noted that the separation of the ashing and electrical heating stages could lead to uncertainties regarding how well the procedure represents the agglomeration process in the actual full-scale combustion process. [93, p. 121]

The samples obtained from lab- and pilot-scale trials can be analyzed with several techniques, including *x-ray diffraction (XRD)* and *scanning electron microscopy (SEM)*. XRD analysis shows the crystalline phases present in the sample. The results can be used to identify the materials responsible for bed agglomeration. However, since XRD only provides the crystalline phases, some of the amorphous binding material may not be identified. SEM analysis methods reveal information about the chemistry, size, shape and number of particles present. *Backscatter electron (BE) images* obtained from morphological analysis show the bonding of agglomerates and point chemical analyses can be conducted to uncover the elements present in selected locations. [70, p. 162–163]

5.2 In-situ monitoring and prediction

The most common in-situ agglomeration monitoring and prediction methods are based on temperature and pressure measurements. In the past years, several other technologies have also been studied, from acoustic emission measurements to fibre optic sensors. More work is still required to find accurate and cost-effective methods. [72, p. 470][12, p. 650–652]

5.2.1 Pressure

Real-time measurement of the pressure drop across the bed is normally used in monitoring fluidization behaviour, hydrodynamics, density and height of the bed. Variety of algorithms and statistical analyses have been applied in the hope of linking the pressure drop to the beginning of agglomeration or defluidization. The problem with pressure drop is that it only represents the bed as a whole, and smaller scale disturbances might be ignored. There is also a chance of inaccuracies caused by probe blockages. Reliable and accurate methods have still not been found. [12, p. 642–650][72, p. 470]

5.2.2 Temperature

As with pressure, temperature measurements are routinely used in fluidized bed boilers to monitor the degree of mixing of the bed [72, p. 470][120, p. 17]. Given the detrimental effect agglomeration has on mixing, temperature peaks could be used to indicate the onset of agglomeration or defluidization. However, as the temperature effects are only a consequence of the lack of mixing, the usefulness of this method depends on the required warning time. [12, p. 652–654] Another problem with using temperature to predict agglomeration is getting a representative measurement of the whole bed with a finite number of thermocouples [120, p. 17–18]. Additionally, it can be difficult to distinguish temperature peaks caused by normal variation from those caused by agglomeration. [72, p. 470]

5.2.3 Gas-phase alkali components

Some researchers have tried using measurements of gaseous alkali metal components to predict agglomeration. However, the presence of these gas-phase components is not conclusive evidence of agglomeration problems, since other phases are also relevant. Another issue with this prediction method is that proposed technologies only measure the alkali concentration above the bed, when a reading within the bed would be more valuable. Measurements of gaseous alkali compounds could still yield valuable information about agglomeration mechanisms. [12, p. 654]

6 EXPERIMENTAL METHODS

An experimental campaign was carried out to investigate the effect of using alternative bed materials on bed agglomeration with different fuels. The following methods were used:

1. Bed sampling versus operational time during combustion experiments with a lab-scale BFB reactor.
2. Inspection of selected samples to determine the compositions of particle coatings and agglomerate bonds.

This chapter presents the equipment, process parameters, fuels and bed materials used in the combustion trials, as well as the analysis techniques employed to study the bed samples.

6.1 Equipment

Bed agglomeration experiments were carried out with a lab-scale BFB reactor at Valmet Technologies Inc. R & D Center Messukylä. The main chamber of the reactor contains the fluidized bed and has a rectangular cross-section, whose inner side measures about 100 mm. A portion of the bed material stays in place inside a conical enclosure at the bottom of the bed section without being fluidized. The top lid of the chamber has a window, which can be used to monitor bed behaviour.

The possible fuel input range for the reactor is 15–30 kW. Electrical heating elements are used to heat the reactor to the combustion temperature. Fluidization gas is supplied via two perforated tubes at the bottom of the bed. Combustion temperature is controlled by varying the relative fractions of nitrogen and air in the fluidization gas flow. Temperature and pressure probes are located in different parts of the reactor to enable online monitoring of these parameters.

6.2 Process parameters

The main experiments were carried out in the temperature range of 800–850 °C. For some of the more difficult fuels, lower temperatures were also tested. Fuel feeding was started, when the bed temperature reached a value of about 640–700 °C. The mass of the fluidized bed was 2.5 kg. Fluidization gas flow was adjusted to a constant value between

0.9–1.15 m/s for each test in order to operate below the desired temperature limit. Bed load was normally kept constant for each fuel-bed material combination, but some of the fuels required control through the change of fuel feed. Because of the challenging fuels and the small scale of the reactor, it was not possible to maintain constant levels of excess oxygen or environmental pollutants in the flue gases.

Out of the different testing methods presented in chapter 5, the defluidization time method was chosen because of its familiarity and suitability for the experimental reactor. Operation for each combination of bed material and fuel was carried on until defluidization occurred, or at most 16 hours. During longer tests, the reactor was cooled down at the end of the day and started up again on the next test day, without removing the bed. Bed samples were taken every 4 hours of test time and at the time of defluidization. During sampling the fuel feeding was stopped, and about 30 g of sand was removed from the bed through the lid at the top of the reactor chamber by a sampling cup. Defluidization was detected from erratic behaviour of the bed temperature and visual observation through the chamber window. Another confirmation was obtained from the presence of agglomerates in the bed sample taken at defluidization.

6.3 Fuels

Table 6.1 shows the compositions and heating values of the four different fuels used in the experiments. The fuels were selected based on the different characteristics of their ash-forming matter. *Pine bark* was included as a relatively easy fuel, with a low fraction of ash-forming elements, moderate potassium and high calcium concentration. Based on the composition, coating-induced agglomeration was expected to be the dominant agglomeration mechanism. The elevated amounts of Si and Al in the ash were assumed to be from contaminants, such as sand and clay. The fuel had a relatively high moisture content, but combustion experiments were still expected to go smoothly and provide a baseline for the more difficult fuels. The fuel dried during the experimental campaign and in the latter test the moisture content was 35 wt–%.

Tropical wood represented a more difficult fuel in the category of woody fuels, with its high alkali metal concentration. After analysis it was revealed that tropical wood actually contained a relatively low fraction of ash-forming matter, so it was not clear how challenging the fuel would be in regards to agglomeration. The low fraction of Si and the high calcium concentration lead to the assumption that this fuel would also follow the coating-induced agglomeration mechanism.

Oil palm empty fruit bunch (EFB) is a residual husk left over after the palm oil extraction process [25, p. 738]. It was included as an example of a fuel with a considerably high alkali metal concentration, moderate Si content and a low fraction of alkaline earth metals. It was not known, which portion of the silicon concentration resulted from contamination with external mineral matter. The fuel also had the highest ash concentration among the fuels that were tested. Major problems were expected during combustion and the relative

Table 6.1. *Compositions and heating values of the fuels used in the experiments. Abbreviations HHV and LHV denote higher and lower heating value, respectively.*

Fuel	**Bark**	**Tropical wood**	**EFB**	**Bark + EFB blend**	**Straw**
Moisture content (wt–%)	45.3 (35)*	7.2	10.3 (30)**	(33.7)**	8.2 (30)**
Ash (wt–% of dry matter)	2.4	0.7	8.9	4.2	8.5
HHV, dry (MJ/kg)	21.2	19.8	18.6	20.5	17.9
LHV, dry (MJ/kg)	20.0	18.5	17.4	19.3	16.7
LHV, wet (MJ/kg)	9.8	17.0	11.4	11.9	11.0
Elemental composition, wt–% of dry matter					
C	54.6	50.6	46.3	52.3	45.1
H	5.7	5.9	5.4	5.6	5.5
O	37.4	42.6	37.4	37.0	44.1
N	0.40	0.26	1.2	0.62	0.59
Cl	0.01	0.049	0.53	0.15	0.27
S	0.03	0.02	0.16	0.066	0.08
Ash-forming element composition, wt–% of dry matter					
Si	0.12	0.01	0.99	0.36	2.4
Al	0.08	$<$ 0.001	0.05	0.073	0.09
Fe	0.02	0.002	0.08	0.039	0.05
Ca	0.54	0.13	0.38	0.50	0.51
Mg	0.05	0.02	0.22	0.099	0.10
Na	0.02	0.03	0.04	0.021	0.05
K	0.16	0.13	2.80	0.89	1.1
P	0.04	0.02	0.14	0.065	0.10
Ash-forming element composition as oxides, wt–% of ash					
SiO_2	10.70	1.80	23.79	18.41	59.90
Al_2O_3	6.38	$<$ 0.27	1.11	3.30	1.91
Fe_2O_3	1.37	0.49	1.31	1.34	0.89
CaO	31.48	25.99	5.90	16.53	8.40
MgO	3.66	4.97	4.08	3.92	1.95
Na_2O	0.84	6.16	0.55	0.67	0.71
K_2O	8.03	22.37	37.71	25.48	15.16
P_2O_5	3.44	6.22	3.59	3.54	2.70

* The fuel had dried to the value given in brackets for the latter test.

** These fuels were moisturized to the value given in brackets.

effect of coating-induced and melt-induced mechanisms was a point of interest. The fuel was available as excessively hard pellets. To improve the compatibility of this fuel with the lab-scale reactor, the pellets were softened by adding water and sieved to remove the finest particle fraction.

Wheat straw was selected to represent an agricultural fuel with a high concentration of reactive Si, low calcium content and a high fraction of ash-forming matter. The alkali metal content was also high, although not as high as in EFB or tropical wood. Based on previous studies [16, p. 830–831], the high reactive silicon in the presence of alkali met-

als was expected to result in fast defluidization through the melt-induced agglomeration mechanism. This fuel was also obtained as pellets, and a treatment similar to the one used for EFB was applied.

As a final test, a blend of 75 wt–% of pine bark and 25 wt–% of EFB was tested. The purpose of this mixed fuel test was to further study the effect of different proportions of reactive silicon, alkali metals and calcium in the fuel. The blend was prepared simply by mixing the fuels by hand. The resulting mix was not entirely homogeneous, but this was assumed to have no significant effect on the accumulation of ash matter in the reactor.

6.4 Bed materials

Table 6.2 shows the size information and elemental compositions for the four bed materials used in the tests. For GR Granule (GRG) the size range was obtained from the bed material supplier. The other size ranges were determined by sieving. The sieve sizes used were 0.63 mm, 1 mm, 1.6 mm and 2.5 mm. The average size and variance were estimated based on the sieving results. The compositions were obtained from *x-ray fluorescence (XRF)* analyses conducted by Satu Ilvonen at Eurofins Expert Services Inc. laboratory in Otaniemi. Similarly to the fuel table 6.1, the oxides in table 6.2 are not actual compounds detected in the material, but rather just a common way to present elemental composition.

Table 6.2. *Some properties of the bed materials used in the experiments.*

Bed material	**Quartz**	**Natural sand**	**GRG**	**Diabase**
Size range (mm)	0–1	0.63–1.6	0.5–1.2	0–1.6
Estimated average size (mm)	0.75	0.84	0.94	1.0
Estimated variance (mm^2)	0.03	0.12	0.09	0.11
Composition, wt–%				
Si	46	39	16	21
Al	0.28	4.7	5.8	9.6
Fe	0.03	0.94	1.1	11
Ca	0.03	0.43	24	5.9
Mg	$<$ 0.01	0.33	6.7	3.5
Na	0.02	1.2	0.47	2.4
K	0.14	3.1	0.84	1
P	$<$ 0.01	0.05	0.01	0.26
Composition as oxides, wt–%				
SiO_2	98.4	83.4	34.2	44.9
Al_2O_3	0.53	8.88	11.0	18.1
Fe_2O_3	0.04	1.34	1.57	15.7
CaO	0.04	0.60	33.6	8.26
MgO	$<$ 0.02	0.55	11.1	5.80
Na_2O	0.03	1.62	0.63	3.24
K_2O	0.17	3.73	1.01	1.20
P_2O_5	$<$ 0.02	0.12	0.02	0.60

Since quartz particles are known to participate in the mechanism of coating-induced agglomeration, the four bed materials were chosen based on their quartz content. The Eurofins Expert Services laboratory performed XRD analyses to identify the crystalline compounds in each bed material. The *quartz* bed material consisted almost exclusively of quartz particles, aside from small amounts of impurities. This type of bed material represents the sand occurring naturally in some parts of the world [60, p. 4]. The material called *natural sand* also contained primarily quartz, but also K- and Na-feldspars. This type of sand more accurately represents the bed materials used in commercial boilers in Skandinavia [31, p. 1343].

For comparison, two quartz-free bed materials were tested, *GR Granule (GRG)* and *olivine diabase*. For these materials, no adhesive coating formation was expected during combustion. GRG is a new bed material produced from crystalline *blast furnace slag (BFS)*. It differs from previously used amorphous BFS by its structure and particle morphology. GRG mainly consisted of calcium, magnesium and iron silicates. Based on the XRD analysis, the olivine diabase bed material contained some plagioclase feldspars and other more complicated silicate minerals.

6.5 Bed sample analyses

The Eurofins Expert Services Inc. laboratory provided various chemical analyses and images of the bed samples taken during the experimental campaign. The bulk elemental compositions were determined using x-ray fluorescence (XRF) analysis. Additionally, selected samples were embedded in epoxy resin and then cut and polished for photography of the cross-sections through a stereo microscope. These cross-sections were also observed by *scanning electron microscopy (SEM)* and subjected to *energy-dispersive x-ray spectroscopy (EDS)* analysis to obtain maps showing the relative concentrations of different elements. For each sample, the bridges between attached particles were analyzed separately to yield approximate elemental compositions at discrete locations.

7 RESULTS AND DISCUSSION

This chapter presents the results of the experimental campaign. In the first section, the general progress of the tests is reviewed and primary results for each of the fuels are stated. Next, some attention is given to different types of agglomerates found in the samples and the relative accumulation of alkali metals in different bed materials. Finally, some overall findings are discussed.

7.1 Defluidization time and coatings

The combustion experiments can be compared based on the defluidization times for different combinations of bed material and fuel, shown in tables 7.1–7.3. Not all tests resulted in defluidization in the maximum test time, as seen from the shutdown reasons for each test. The temperature range for each test is expressed in terms of an upper limit and a temporal average. The difference between average values in tests with the same upper limit was not very large. The cumulative alkali metal feed is calculated from the fuel feed mass flow and the concentration of alkali metals in the fuel. It is not known what portion of the fed amount stays in the bed and how much is released to the flue gases.

In addition to the defluidization times, bed materials were compared by observing the extent and compositions of the coatings on their surfaces in scanning electron microscopy (SEM) images. The grayscale backscatter electron (BE) images show materials of higher atomic weight in a brighter colour. This makes it possible to identify different minerals from the images. The minerals were even more recognizable from the multi-colored elemental maps created with EDS. However, these images were quite large, so they were left out of this chapter.

7.1.1 Bark

Table 7.1 shows the test results for bark. The tests progressed without defluidization until the maximum test time of 16 hours. Controlling the combustion process was relatively easy, except for occasional plugging of the fuel feeding tube. There were barely any signs of fouling in the furnace. Only a few isolated agglomerates were seen in the bed samples during testing of both GR Granule (GRG) and quartz. Subsequently, it was decided that natural sand would not be tested, since based on quartz content, it would only be a less severe version of the quartz case and a limited amount of time was available.

Table 7.1. *Test results for bark.*

Bed material	Temperature, upper limit [°C]	Temperature, average [°C]	Fuel feed, average [g/s]	Cumulative alkali feed [g]	Duration [h]	Shutdown reason
Quartz	850	830	1.2	69	16	Planned
GRG	850	828	1.2	73	16	Planned

The SEM backscatter electron images presented in figure 7.1 show a clear difference between bed particles in quartz and GRG tests. Quartz particles are covered in continuous coatings (figure 7.1 a), while no such coatings are observed for GRG particles (figure 7.1 b). The few, small agglomerates found were formed mainly around quartz particles in both tests. The quartz particles found in the GRG samples probably originate from the fuel. They can be identified from figure 7.1 b by their darker color, since they have a lower atomic weight than GRG particles. A few GRG particles had also been glued together by narrow bridges that were probably caused by the melt-induced mechanism.

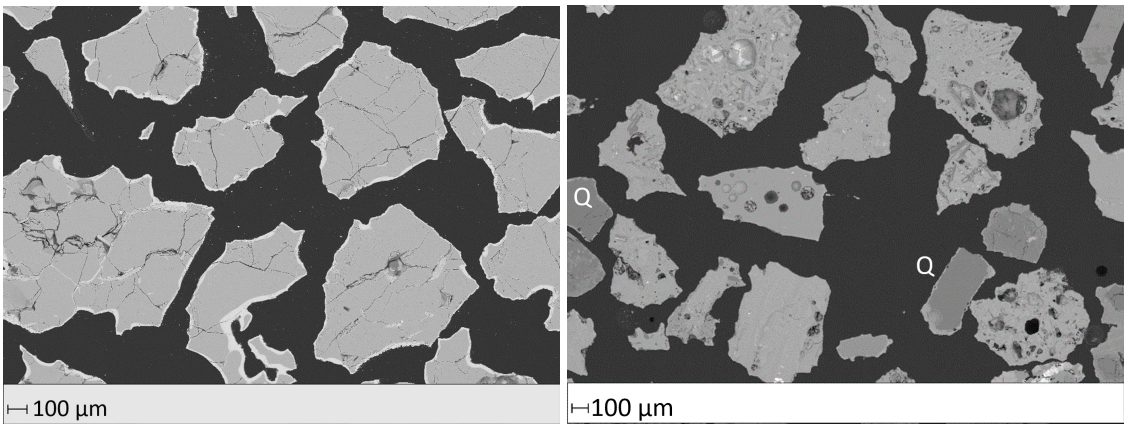

(a) ***(b)***

Figure 7.1. *SEM BE images of samples from the bark tests using (a) quartz and (b) GR Granule as bed material. Quartz particles in figure (b) are denoted by "Q".*

The sample from the bark test using quartz bed material was chosen to further investigate the coatings on quartz particles. Figure 7.2 shows a close-up BE image of the coating and compositions at different locations obtained from EDS analysis. The coating consists of two distinct layers.

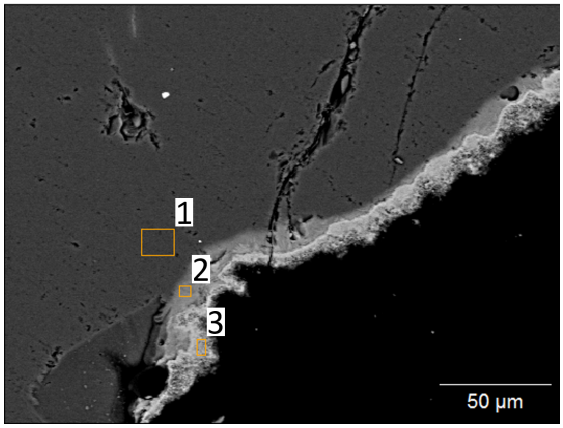

	1 [wt–%]	2 [wt–%]	3 [wt–%]
O	53.4	42.7	39.6
Na	0	0.7	0
Mg	0	0.8	7.1
Al	0	0	4.6
Si	46.6	36.0	6.9
K	0	13.2	1.3
Ca	0	6.1	33.4
P	0	0	4.9
Fe	0	0	0.8

Figure 7.2. *A close-up BE image of the coating on a quartz particle in a sample from the bark-quartz test and compositions in different points obtained from EDS analysis.*

Apart from oxygen, the inner layer consists almost entirely of Si, K and Ca. The outer layer composition is more diverse and also contains a significant amount of Mg, Al and P. Potassium and silicon are clearly enriched in the inner layer, whereas calcium concentration is higher in the outer layer. Based on this one sample, the maximum thickness of the coating seems to be about 25 µm.

7.1.2 Tropical wood

The dry tropical wood reacted rapidly in the lab-scale reactor and sharp temperature peaks were observed periodically. This made bed temperature control more challenging than in the bark case. As in the bark tests, there were no signs of any significant fouling of the reactor chamber. Table 7.2 shows the test results for tropical wood.

Table 7.2. *Test results for tropical wood.*

Bed material	Temperature, upper limit [°C]	Temperature, average [°C]	Fuel feed, average [g/s]	Cumulative alkali feed [g]	Duration [h]	Shutdown reason
Quartz	850	830	1.4	27	3.0	Defluidization
Natural sand	850	832	1.3	88	12.5	Defluidization
GRG	850	834	1.3	116	16.0	Planned

Because of the high fraction of fine matter in the fuel, a relatively low fluidization velocity was used as an attempt to prevent excessive fuel carry-on from the bed. All the tests were conducted in the high-temperature range of 800–850 °C. Tests in reduced temperatures would have also been interesting, but not enough fuel was available.

The quartz test ended in only 3 h, while the test with GRG lasted until the maximum test time without defluidization. At about 10 h of test time in the natural sand test, a malfunction in the nitrogen generator caused a temperature peak, which was falsely interpreted as a sign of defluidization. The bed had already been removed, when the mistake was noticed. The experiment was resumed about a month later with the same bed material,

until defluidization in 12.5 hours of test time. During bed removal, the inert, not fluidized bed was mixed into the active bed, diluting the bed somewhat in regards to alkali metal content. It is possible that this procedure delayed defluidization to some extent. However, this effect was apparently not very large, since defluidization was still observed in only 2.5 hours after continuing the test.

In all three test cases the SEM images show coatings mainly around quartz particles (figure 7.3).

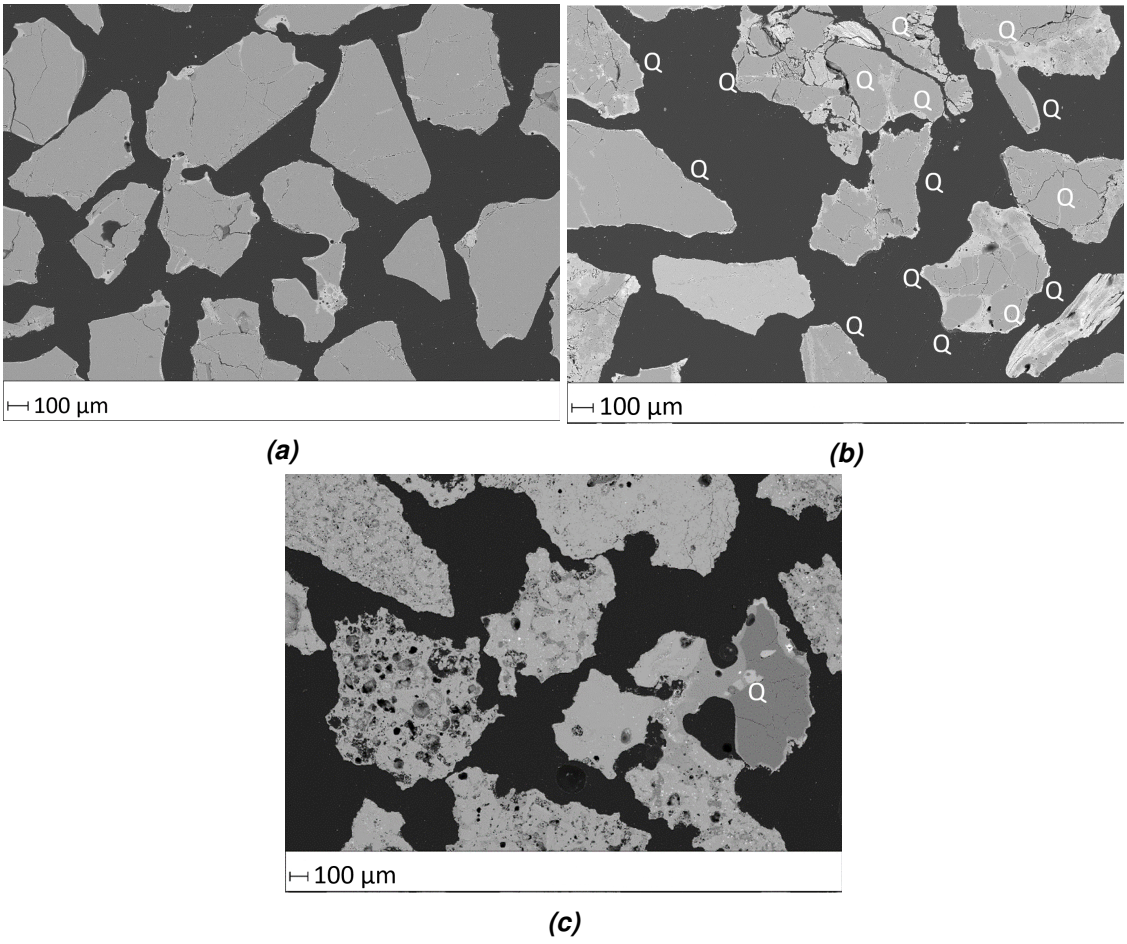

Figure 7.3. *SEM BE images of bed particles from the tropical wood tests using (a) quartz, (b) natural sand and (c) GR Granule as bed material. Quartz particles in figures (b) and (c) are denoted by "Q".*

In the natural sand test, coatings could also be seen on feldspar particles, but they were much thinner and more discontinuous in comparison. As in the bark tests, quartz particles were also found among GRG samples.

7.1.3 EFB

In empty fruit bunch (EFB) tests the control of the combustion process became noticeably more challenging. In spite of the softening and sieving treatment of the pellets, some large fuel particles remained among the fuel. These particles combusted very slowly and

stayed in the bed for long periods of time. As a result, the entire bed could be covered by the burning pellets, causing defluidization in a way, which had nothing to do with bed agglomeration. The issue was solved by decreasing the bed load significantly through reduced fuel feed. Deposits started to form on the walls of the reactor chamber very quickly after the fuel feeding was started. However, based on bed samples and visual observation from the chamber window, it was concluded that slag was not falling to the bed in excessive amounts and tests could be resumed.

Table 7.3 shows the results for EFB. High-temperature tests with all the bed materials ended in less than an hour as a result of defluidization. Since the high-temperature tests were so short, some tests in reduced temperatures were also conducted, to study the importance of the bed temperature on agglomeration. However, the low-temperature tests showed barely any signs of agglomeration, so they were often concluded even before the approved maximum test time of 16 hours to save time.

Table 7.3. *Test results for EFB.*

Bed material	**Temperature, upper limit** [°C]	**Temperature, average** [°C]	**Fuel feed, average** [g/s]	**Cumulative alkali feed** [g]	**Duration** [h]	**Shutdown reason**
Quartz	850	821	0.6	31	0.5	Defluidization
Quartz	800 → 850*	798 → 828	0.8	239 → 398	4.5 → 2	Defluidization
Quartz	800	783	0.5	190	5.0	Planned
Quartz	750	731	0.5	313	8.0	Planned
Natural sand	850	824	0.6	13	0.2	Defluidization
GRG	850	821	0.5	40	0.8	Defluidization
GRG	800	783	0.5	341	8.0	Planned
GRG	750	731	0.5	624	16.0	Planned
Diabase	850	820	0.7	30	0.5	Defluidization

* Test was started with upper temperature limit of 800 °C and changed to 850 °C after 4.5 h.

An interesting observation was made in the quartz test with upper temperature limit of 750 °C. The bed particles had a recognizable black coating, which could have consisted of soot or a product of some reaction occurring in lower temperature combustion. Yet no agglomeration was detected in this test, so the samples were not included in the SEM-analyses.

One quartz test was conducted in two stages. It was started by using the upper temperature limit of 800 °C. Based on the bed sample it seemed that agglomeration would not proceed in this temperature range, so the test was continued with 850 °C as the upper temperature limit. Surprisingly, defluidization took longer in the high-temperature area in this test, than in the quartz test, which was started at the higher temperature. To the author's knowledge, tests like this have not been conducted previously, so explanations cannot be found from other studies. Perhaps the high amount of solid ash formed in the lower temperature phase in the bed and the walls diluted the melt, which formed after the temperature was raised, and decreased its ability to form agglomerates.

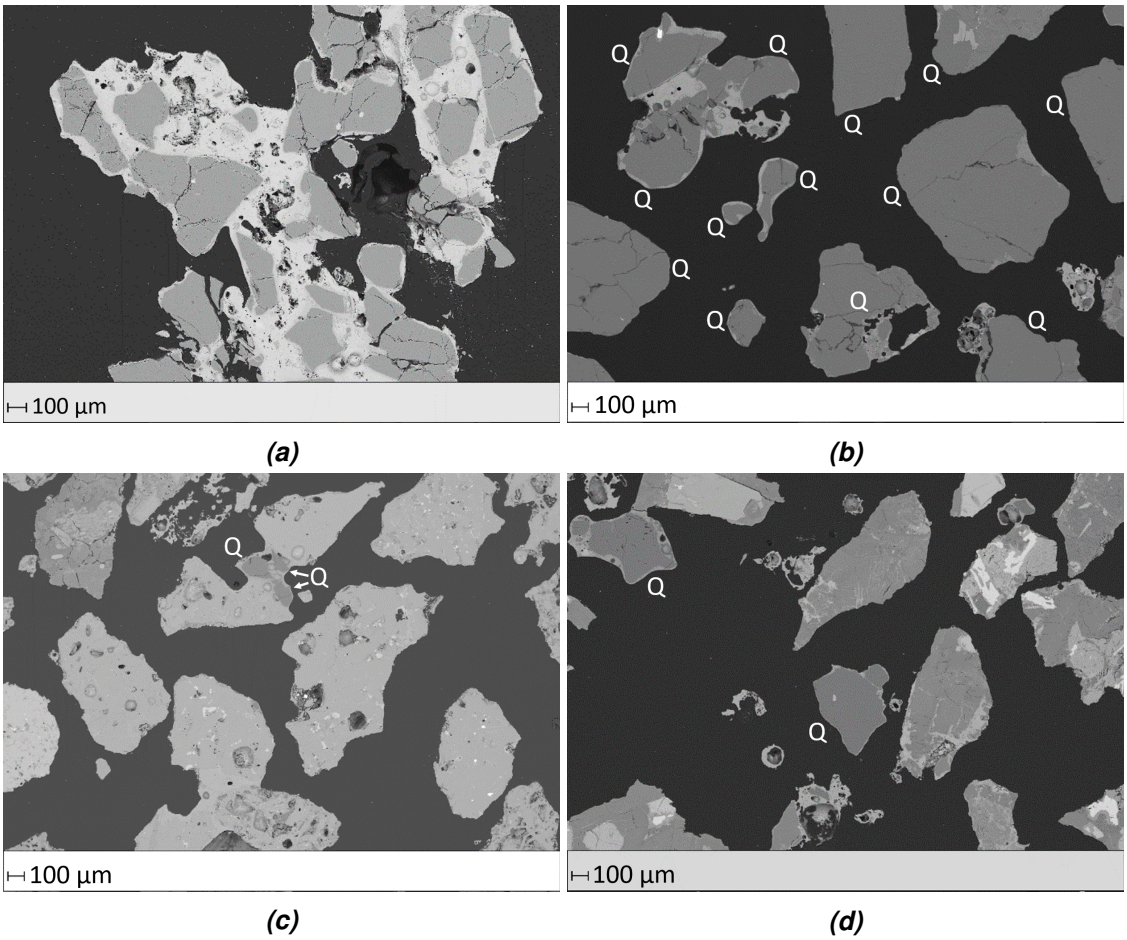

Figure 7.4. *SEM BE images of bed particles from the EFB tests using (a) quartz, (b) natural sand, (c) GR Granule and (d) diabase as bed material. Quartz particles in figures (b), (c) and (d) are denoted by "Q".*

SEM BE images were produced for samples from the tests using the higher temperature limit of 850 °C (figure 7.4). All the samples included multiple agglomerates glued together either by an ash melt or by the coatings on quartz particles. As in other tests, distinct alkali silicate coatings were only found on quartz particles. GRG and the feldspars present in natural sand did not show coatings. The only diabase sample sent to SEM analysis in this thesis was the one from the high-temperature EFB test. It was confirmed that diabase particles also showed no coatings and agglomerates in the sample were centered around quartz particles.

7.1.4 Bark + EFB mixture

The test with the bark-EFB fuel blend was conducted in an average temperature of 830 °C with 850 °C as the upper temperature limit. The bed samples showed no signs of agglomeration, so due to the limited time available, the test was concluded without defluidization after 8 hours of combustion. The cumulative alkali feed at the time of termination was 210 g. The SEM images seemed very similar to the ones from bark combustion with a quartz bed. Continuous coatings could be found on quartz particles and several agglom-

erates were present, attached together by either the coatings or an ash-derived melt.

7.1.5 Straw

In the tests with the straw pellet fuel, the fouling of the reactor chamber was even more severe than in the EFB tests. It was not possible to determine, whether the chunks of ash in the bed resulted from bed agglomeration or had fallen from the slag-covered reactor walls. Perhaps as a result of the slagging, maintaining the high temperature during tests proved impossible, even after improved fuel sieving. From the beginning of fuel feeding, the temperature started to decrease steadily. The lower temperature limit of 750 °C was tested, and this way fouling and temperature control were manageable. However, it seemed that agglomeration would not proceed at all in this temperature, and no useful results would be obtained.

Due to these problems, combustion of straw was discontinued after a few tests, and the lab-scale reactor was deemed unsuitable for this fuel. Therefore, no results can be presented from the straw tests.

7.2 Agglomerates

Based on the literature review, it was expected that the agglomerates found in the test samples were formed by either the coating-induced or melt-induced mechanism. No quantitative method exists for identifying the different mechanisms from particle bridge compositions. However, a qualitative categorization can be achieved by assuming that the agglomerates that show distinct coatings on the attached particles have resulted from the coating-induced mechanism and the ones without coatings are bound by an ash melt. In the samples the former case was usually observed with quartz particles and the latter with quartz-free materials. Some agglomerate bonds were also observed between quartz and either GRG or diabase particles. In this case it seemed that the bond was caused by the alkali coatings on quartz particles, since the compositions were similar to the bonds between quartz particles.

7.2.1 Coating-induced agglomerates

Figure 7.5 shows an example of an agglomerate bridge between two coated quartz particles from the test conducted for bark and quartz. The accompanying table shows the bridge composition at different points, acquired from EDS analysis.

The main elements (excluding O) found in coating-induced agglomerate bonds were Si, K and Ca. The bridge compositions were not spatially uniform, but varied in a broad scale. Generally, it seemed that the mass fraction of silicon decreased towards the center of the bond, whereas that of calcium increased, as seen in figure 7.5. No similar spatial relation was found for potassium in the results, its concentration seemed to vary randomly.

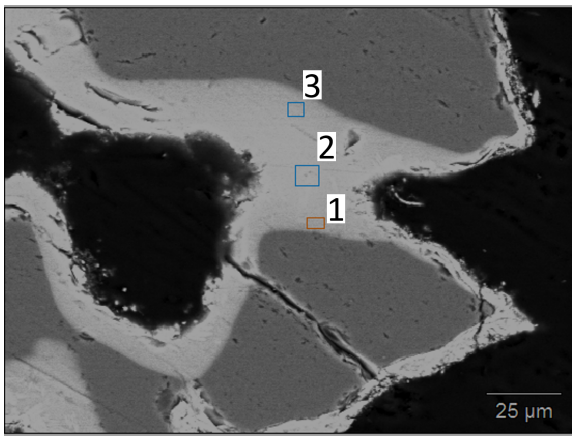

	1 [wt–%]	2 [wt–%]	3 [wt–%]
O	43.5	40.6	42.2
Na	1.0	1.3	1.1
Mg	0.5	0.6	0.3
Al	-	0.7	-
Si	34.2	28.9	33.5
K	15.6	17.7	17.5
Ca	4.7	9.6	5.0
Mn	0.5	0.6	0.4

Figure 7.5. *A SEM BE image of a bridge between two quartz particles in a sample from the bark-quartz test and compositions in different points obtained from EDS analysis.*

Depending on the fuel, other elements were also present in elevated concentrations. The fractions of different elements seemed to mirror the differences between fuel ash compositions. For example, the bridges in tropical wood cases contained between 3–14 % Na, while for the bark tests the corresponding range was 1–3 %. Similarly, in the test with the blend of EFB and bark, the melt contained less calcium than in the case with pure bark.

Some bed particles included cracks that could have been formed through the crack layer formation mechanism, as in the lower particle in figure 7.5. However, it is equally possible that there were two separate particles present originally, especially since the crack is not entirely filled with the alkali silicate melt, as in the figures of He et al. [50]. Also, based on the mechanism they proposed, crack layers were not expected to form in these relatively short tests. Still, the process conditions and the fuel in this thesis are different from the ones they used, which could cause the difference in formation time.

7.2.2 Melt-induced agglomerates

Figure 7.6 shows an example of an ash melt bridge between two GRG particles in a sample taken from the EFB-GRG test and compositions at different locations. The melt-induced bridges seem to have a more diverse composition than the coating-induced ones. In addition to Si, K and Ca there are significant amounts of other elements present, including Mg, P and Fe. Based on the EDS analysis in figure 7.6, the bridge is also more homogeneous in regards to composition in the different parts of the bridge. For example, Si is not as noticeably enriched in the area near the particles, as was observed for the quartz particles. However, the difference is not very large and the larger concentrations of the other elements might be part of the reason.

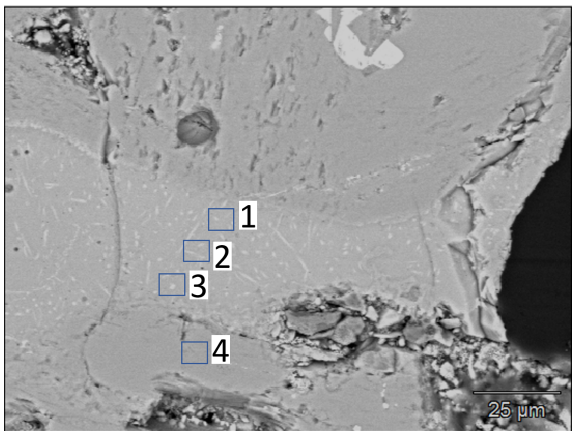

	1 [wt–%]	2 [wt–%]	3 [wt–%]	4 [wt–%]
O	38.9	39.9	38.4	41.1
Na	1.9	1.5	1.7	0.5
Mg	4.4	4.7	5.1	5.9
Al	1.0	0.8	1.1	6.3
Si	19	18.2	19.4	17.7
P	2.1	2.7	1.8	-
S	-	-	0.3	-
K	20.6	18.1	20.3	0.4
Ca	8.6	11.9	9.3	28.3
Fe	3.5	2.3	2.6	-

Figure 7.6. *A bridge between two GRG particles in a sample from the EFB-GRG test and the composition in different points obtained from EDS analysis.*

The melt-induced bond in figure 7.6 contains small, string-shaped areas scattered throughout it. They seem to be mainly composed of phosphorus and calcium. The cause of these discrete areas is unknown. Perhaps they are solid, high-melting-point calcium phosphate particles mixed in the EFB ash melt.

7.2.3 Quantitative categorization of agglomerates

In the literature it has been stated that the composition of melt-induced agglomerate bridges more closely resembles the global ash composition of the fuel, compared to the coating-induced bridges [39, p. 932]. This seems reasonable, since the bridges are formed directly from molten ash. If this notion was quantified, it could be used to identify the dominant agglomeration mechanism from agglomerate bridge compositions. To this end, the *root-mean-square errors (RMSE)* for each agglomerate bridge composition were calculated in comparison to the global ash composition.

The RMSE is a common measure used to quantify the effectiveness of a model. For model values $\hat{\theta}$, it is calculated from $RMSE = \sqrt{1/\mathbf{n}\sum_{i=1}^{\mathbf{n}}(\theta_i - \hat{\theta}_i)^2}$, where $\mathbf{n}$ is the number of model predictions and θ is the observed value of the variable being predicted. [23] In this case the fuel ash composition is considered as a model predictor for the agglomerate bridge composition and the model predictions are the mass fractions of different chemical elements. Consequently, bridges formed through the melt-induced mechanism should have a relatively low RMSE value. Oxygen was excluded from the agglomerate bridge compositions to make comparison to fuel ash composition possible. The resulting RMSE values are plotted in figure 7.7.

The RMSE values did not predict the agglomerate mechanism very consistently. For bark and tropical wood samples, the values for the bridges involving quartz are larger, but in some cases the difference is only a few weight percent. The results for EFB tests are even less reasonable. For example, the sample from the bark-EFB blend combustion with quartz sand as bed material has a relatively low RMSE value, even though the presence of coatings would indicate coating-induced agglomeration mechanism to dominate.

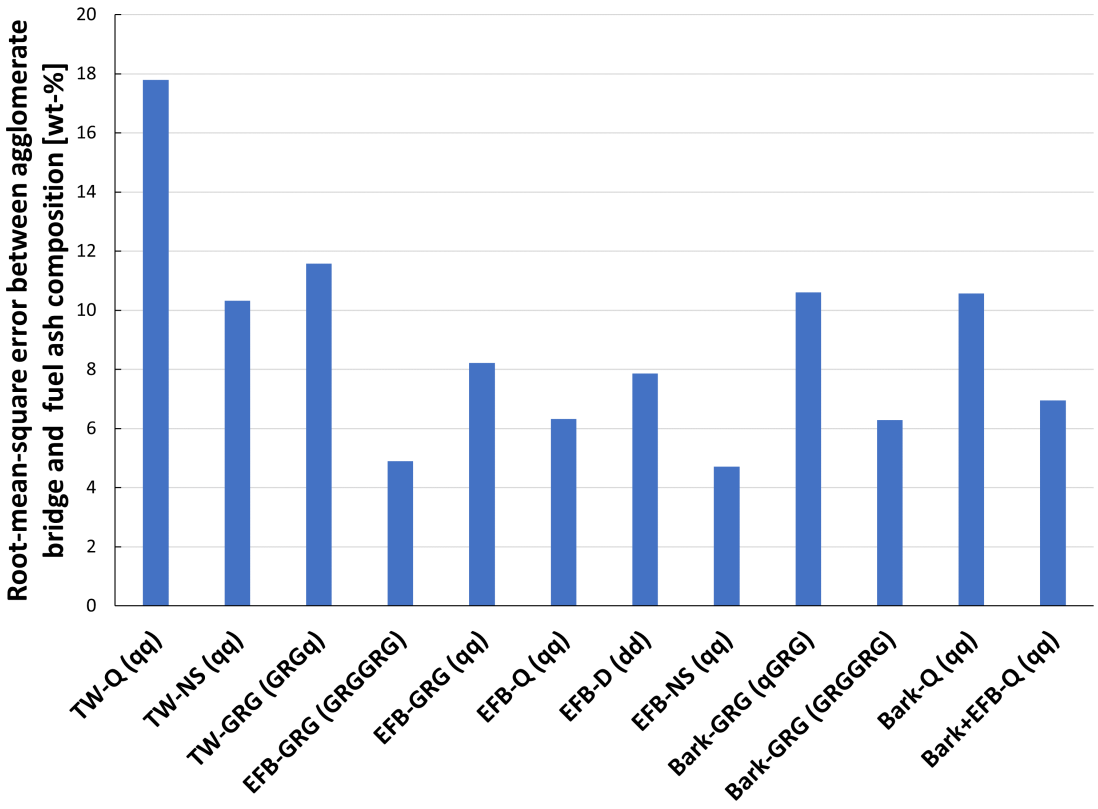

Figure 7.7. *The root-mean-square errors between fuel ash and agglomerate bridge compositions for bridges in different samples. The letters in brackets indicate, which two particles were held together by the bridge. The meaning of the acronyms: TW = tropical wood, Q = quartz, NS = natural sand, GRG = GR Granule, EFB = empty fruit bunch, D = diabase.*

Similar graphs with only some of the ash elements included were also created, but the outcome was not any better. Perhaps a better result would have been acquired with more samples or a larger amount of agglomerate bridge analyses from each sample. It should also be noted that the SEM analysis only inspects a single 2-dimensional projection of the binding bridge, so it might not be completely representative of the entire thickness.

7.3 Alkali metal accumulation

As part of the comparison of different bed materials, the accumulation of alkali metals in bed samples was investigated by comparing the x-ray fluorescence (XRF) analyses of unused bed materials and samples taken during the tests. Figure 7.8 shows the relative increase in the mass fraction of alkali metals Na and K found in quartz and GRG bed samples during bark tests.

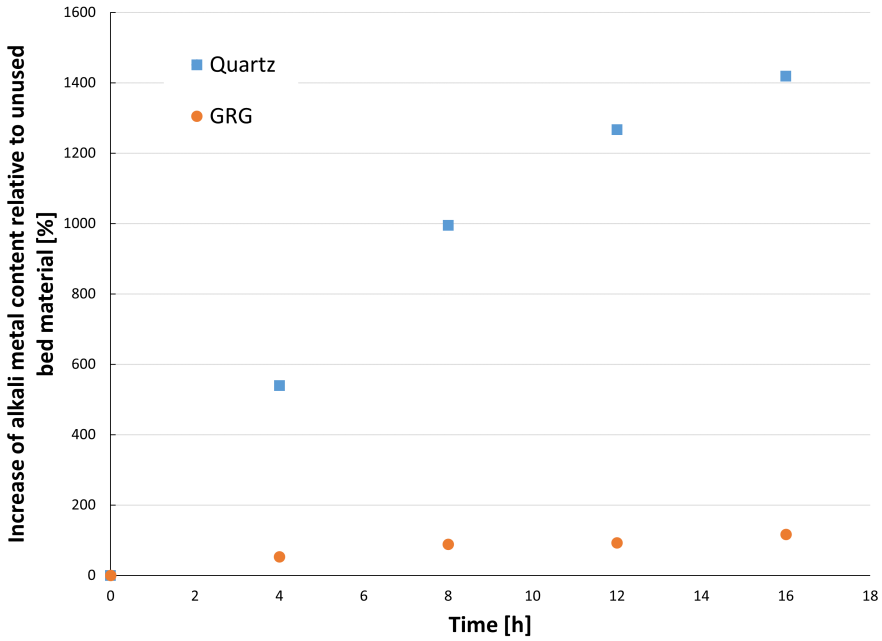

Figure 7.8. *Accumulation of alkali metals for quartz and GRG bed materials in the bark tests.*

A distinct difference can be seen between the bed materials in their tendency to store alkali metals. After 16 h the alkali content of quartz has increased 15-fold, while that of GRG has only doubled. Nevertheless, the alkali content of the GRG samples is increasing steadily. Figure 7.9 plots the accumulation of alkali metals for natural sand and GRG in tropical wood combustion.

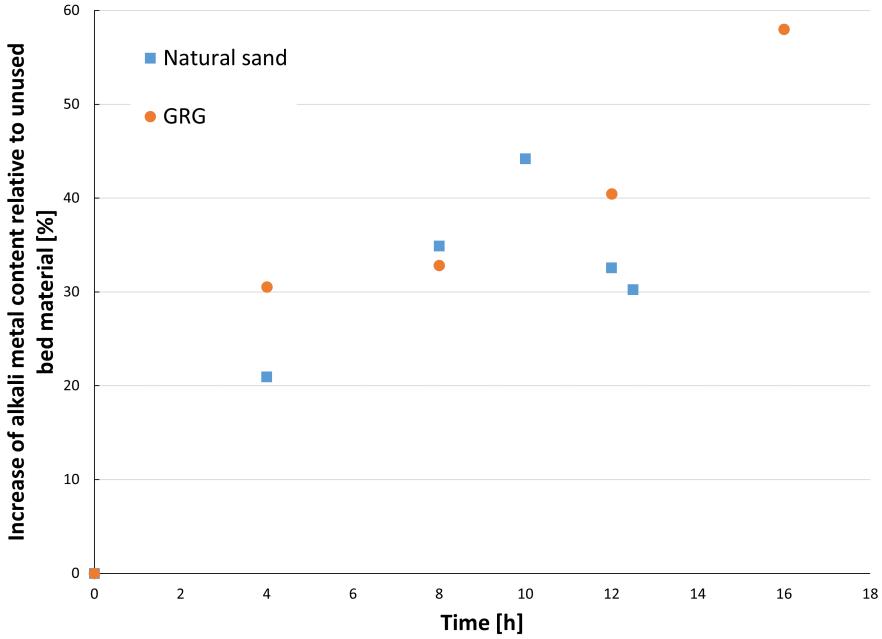

Figure 7.9. *Accumulation of alkali metals for natural sand and GRG bed materials in the tropical wood tests.*

Quartz was left out of the chart in figure 7.9 for clarity, since it increased to about 550 %

after 3 hours, confirming its high tendency to store alkali metals. Natural sand seems to surpass GRG in alkali accumulation after about 8 h of operation. The later drop in the alkali content of natural sand is the result of the bed removal discussed in subsection 7.1.2. When the bed was removed, it was mixed with the inert, unused bottom part of the bed, which is not included in the previous bed samples. Subsequently, the relative amount of pure quartz increased at the expense of the alkali metal concentration. Therefore, the last two values for natural sand are not comparable to the previous ones. It is surprising that a lower accumulation value for GRG was obtained for the tropical wood test, which had a higher cumulative alkali feed (table 7.2). It is possible that this is caused by the different ash formation reactions of the two fuels, since they determine, which portion of the alkali metals stays in the bed.

Table 7.4 shows the accumulation of alkali metals in the high-temperature EFB tests. These tests were so short that no samples were taken before defluidization and a scatter plot would have been redundant. When comparing the alkali accumulation values in the table, it should be done for the same cumulative alkali feed between cases to obtain a reliable approximation of the alkali affinities. However, this would require interpolation of the alkali metal fractions and the accuracy would be questionable. Nevertheless, some conclusions can be made from the table, while accounting for both the alkali metal feed and accumulation values.

Table 7.4. *Total relative increase of alkali metals in the high-temperature EFB tests.*

Bed material	**Cumulative alkali feed**	**Test time**	**Alkali metals, unused bed material**	**Alkali metals, test end**	**Relative increase**
	[g]	[h]	[wt–%]	[wt–%]	[%]
Quartz	31	0.5	0.16	2.65	1577
Natural sand	13	0.2	4.30	5.30	23
GRG	40	0.8	1.31	6.30	381
Diabase	30	0.5	3.40	6.00	76

For the EFB tests the affinity of quartz for alkali metals is again evident. Surprisingly, the lowest increase in alkali metals seems to have occurred for natural sand, even if the low cumulative alkali metal feed is taken into account. GRG in turn reaches a relatively high value. Consequently, the alkali metal accumulation values for EFB seem to be less dependent on the quartz content of the bed materials.

In EFB combustion quartz accumulated significantly more alkali metals than in tropical wood or bark combustion with the same alkali metal feed. A clear difference is also seen for GRG and probably also for natural sand, if the cumulative alkali feed values are taken into account. This could be an indication of the differences in agglomeration tendency and mechanisms for these fuels. Still, when comparing the accumulation values between fuels, it should again be noted that different fuels release different degrees of their alkali content to flue gases and this determines, how much alkali metals are available to accumulate on bed particles.

7.4 Discussion

Based on the results presented in previous sections, the effect of quartz-free bed materials on agglomeration for different fuels can be speculated. For tropical wood, the defluidization time was inversely proportional to the quartz content in the bed materials, indicating that the alternative bed materials were effective in preventing agglomeration. The agglomeration tendency of bark was not high enough to cause defluidization in the test time, so the effectiveness of alternative bed materials cannot be inferred from test durations. Based on literature sources, these two fuels follow the coating-induced agglomeration mechanism. Consequently, it seems likely that quartz-free bed materials inhibit agglomeration from occurring via the coating-induced path. This conclusion is supported by the fact that significant coatings were only observed on quartz particles in all tests. Alkali accumulation charts also indicate that significantly less alkali metals are stored in GRG compared to quartz or natural sand. Nevertheless, agglomerates bound by ash-derived melt were also found in the samples for both of these fuels, so coating-induced agglomeration is not the only mechanism at play.

For EFB, defluidization was observed in about the same time for different bed materials. Based on the conclusions reached for bark and tropical wood, this could indicate that melt-induced mechanism governs agglomeration for this fuel. Coatings of significant thickness were also present on quartz particles, and they took part in agglomerate formation, even in the tests lasting less than 0.5 hours. Yet, the fuel feed flow in the EFB tests was so low that the mass of fuel-derived quartz particles during the entire test was only about 10 g, if all the silicon content in the fuel is assumed to come from them. Therefore, the role of fuel-derived quartz particles in agglomeration is expected to be relatively insignificant. For EFB, agglomeration was also highly dependent on temperature, since defluidization was not achieved in any of the lower-temperature tests. However, temperature-dependence is known to be a property of both the coating-induced and melt-induced mechanisms. Based on these results, it is concluded that agglomeration for EFB primarily follows the melt-induced mechanism.

The results for tropical wood and bark were in line with those for high-calcium wood-derived fuels from other studies. The literature resources studying agglomeration for EFB in FBC do not really speculate on the relative role of different mechanisms. Kittivech and Fukuda [60, p. 9–11] used EFB as a fuel in gasification in the temperature of 750 °C and found that the main mechanism was coating-induced agglomeration, even though melt-induced agglomeration was also observed. They also managed to prevent agglomeration altogether by using dolomite as bed material instead of silica sand. The reason for these different results could be the different gas atmosphere in the gasification reactor. It is also possible that the relative importance of each agglomeration mechanism depends on the bed temperature.

The coating that was chosen for closer inspection consisted of two layers after 16 hours of bark combustion. This means that the second stage of the coating formation model

proposed by He et al. [48, p. 3845–3847] was reached faster than in their study. As expected, the inner layer primarily consisted of Si, K and Ca, whereas the outer layer composition was more similar to the fuel ash composition. Compared to the final coating composition of Visser [112, p. 36] (table 3.1) for example, the calcium concentration in the inner layer is significantly lower as opposed to Si and K concentrations that are higher. This could be because Ca from the outer layer has not yet had time to migrate to the inner layer to a significant extent.

Even though the combustion tests were generally successful, there is still some room for improvement. For example, the bed materials could have been sieved to the same size range to eliminate the impact of different particle sizes, even if it is not very large. The bed material bulk and particle densities could have been measured prior to the experiments. Then, an attempt could have been made to keep the fluidization number constant between tests to remove the influence of fludization velocity. However, this would have been difficult with the most challenging fuels that required a lot of adjustment of the air and nitrogen flow.

8 CONCLUSION

The goal of this thesis was to investigate the effect alternative bed materials have on bed agglomeration in fluidized bed combustion of different biomass fuels. For this purpose, a literature review was conducted to find out the mechanisms of bed agglomeration, their dependence on operational parameters, as well as the methods to monitor and predict the phenomenon. Additionally, combustion experiments were performed with a lab-scale BFB reactor to study the effect of fuel and bed material composition on agglomeration. Four fuels (pine bark, tropical wood, oil palm empty fruit bunch (EFB) and wheat straw) and four bed materials (quartz, natural sand, GR Granule (GRG) and olivine-diabase) were tested for this purpose.

Bed agglomeration is a phenomenon, in which bed material particles in a fluidized bed attach to each other and form larger structures called *agglomerates*. Without preventive measures the agglomerates could increase in number and size and result in full *defluidization*, which is the collapse of the fluidized bed. There is broad agreement among the researchers that bed agglomeration is caused by molten adhesive material in the bed. In this thesis, bed agglomeration was considered from the point of view of *melt formation*, *particle-level agglomeration*, *sintering* and *defluidization*. Outside of this division, *chemical reaction sintering* and *molecular cramming* are also sometimes included in the group of agglomeration mechanisms. They are fundamentally different, since they are not caused by molten ash, and are probably only relevant in the cyclone and return leg of a circulating fluidized bed boiler, when high amounts of S and Ca are present.

Melt formation mechanisms are often divided into *coating-induced* and *melt-induced* agglomeration. The coating-induced mechanism involves ash deposition on the surface of quartz particles and subsequent chemical reaction between quartz, alkali metals and alkaline earth metals. It is considered the primary mechanism in the combustion of high-calcium fuels, like wood. The mechanism results in an adhesive silicate melt coating of multiple superimposed layers. After the first molten layer is formed, the adhesiveness of the coating starts to diminish, as the fraction of alkaline earth metals grows and the melt composition moves into an area of higher melting point temperature. However, bed particles may also contain *crack layers*, in which gaseous alkali metal compounds have diffused and created a melt. These internal layers can break the particle apart after the protective calcium layer has formed and reveal the adhesive parts again, making agglomeration possible.

Melt-induced agglomeration simply refers to bed particles being glued together by molten

ash. The mechanism does not involve continuous coatings, only local bridges. It typically occurs with fuels that contain significant amounts of potassium and inherent, reactive silicon. In another suggested alternative of this mechanism the molten ash is still located on the surface of the fuel particle, when bed material particles adhere to it. This could result in hollow agglomerates with the same shape as the fuel particles.

On the particle scale, the adhesiveness and bonding of melt-covered particles is a consequence of forces arising from *liquid bridges* and *sintering*. When wet particles collide, the viscosity of the melt will reduce their kinetic energy. If all the kinetic energy is dissipated, particles will remain in contact, held by the capillary force. Sintering mechanisms can then strengthen the bonds in the agglomerate. When agglomerates are large enough, they will no longer be held afloat by the fluidization air and fall to the bottom of the furnace, forming a fixed bed. When the collapsed bed grows in size, it will obstruct the path of the fluidization air, which starts to flow through preferential channels in the bed, disturbing mixing. Eventually, the entire bed defluidizes.

Bed agglomeration is affected by a large number of parameters, like bed temperature, fluidizing gas velocity, fuel properties and possible additive materials used. Alternative bed materials were the main focus of this thesis, and it was found that a large array of materials have been previously tested. *Quartz-free bed materials* have been successful in preventing agglomeration in cases where the coating-induced mechanism was prevalent, but to a lesser degree when melt-induced agglomeration dominated.

Monitoring and prediction methods of bed agglomeration can be subdivided into *pre-combustion prediction* and *in-situ monitoring and prediction* methods. Pre-combustion methods include fuel ash tests, empirical and semi-empirical models, as well as lab- and pilot-scale trials. Currently lab- and pilot-scale trials are considered the only reliable method, but they are time consuming and expensive. In-situ methods are used during the operation of the fluidized bed boiler. They are primarily based on temperature and pressure measurements. More work is still required to find cost-effective and reliable methods.

The experimental campaign achieved limited success. For *tropical wood*, the defluidization time was inversely proportional to the fraction of quartz in the bed material. *Bark* tests did not yield similar results, since the agglomeration tendency of the fuel was not high enough to cause defluidization in the short test time of 16 hours. Still, the results for tropical wood imply that quartz-free bed materials are effective for fuels following the coating-induced agglomeration mechanism. This idea was reinforced by the the fact that for all fuels only quartz particles showed distinct alkali silicate coatings and they accumulated significantly more alkali metals during the tests.

For *EFB*, the bed samples included agglomerates caused by coatings along with those formed by ash melt. Even though quartz-free bed materials still had no coatings, they could not prevent or delay defluidization with this fuel. Consequently, it seems reasonable to assume that the melt-induced mechanism governs agglomeration in EFB combustion.

Wheat straw tests were discontinued because of the excessive fouling of the reactor chamber and the fuel was deemed unsuitable for combustion in the lab-scale reactor used. Therefore, no results could be presented from the straw tests.

The results from the experiments are aligned with the theories presented in the literature: using bed materials with less or no quartz will inhibit agglomeration, when the coating-induced mechanism is prevalent. On the other hand, there are fuels for which the choice of bed material does not seem to matter. This is most likely caused by the fact that they primarily follow the melt-induced mechanism. However, more comprehensive studies should be conducted to get more reliable results.

The research base of bed agglomeration already includes an impressive number of theoretical models and experimental studies, but many questions still remain. The theoretical studies in the context of fluidized bed combustion are mainly focused on the melt formation stage of bed agglomeration. This is understandable, since melt formation is the first stage and therefore probably the most important one from the standpoint of preventing the phenomenon. However, it is not inconceivable that a more detailed knowledge of particle-level agglomeration, sintering or defluidization could yield new methods to inhibit or counteract bed agglomeration.

The terminology used in bed agglomeration studies could be clarified. Based on the literature, it seems that terms such as *agglomeration*, *defluidization*, *sintering* and *silicate* are used quite freely and often without definition. The lack of strict definitions prompts confusion and misunderstandings, more so for researchers new to the subject. Especially the various mechanisms associated with sintering should be established in the context of fluidized bed combustion. The relationship between liquid bridges and viscous flow sintering as mechanisms of agglomeration is also unclear, and has received little to no attention in the literature.

The mechanisms of coating- and melt-induced agglomeration appear to be relatively well established, but only in a qualitative sense. In coating-induced agglomeration, the mechanisms of ash transport on bed particles could be studied further to clear up the disagreement over which pathways are relevant. The coating- and crack layer formation mechanisms proposed by He et al. [48][50] should be confirmed and elaborated on in different process conditions. A more detailed description of the melt-induced mechanism involving hollowed out agglomerates would also be useful.

Many practical aspects of bed agglomeration that are relevant for experimental researchers and plant engineers remain relatively vague. For example, there is no generally accepted quantitative way to distinguish the dominant agglomeration mechanism from bed samples. The only such method found in the literature was the one used by Piotrowska et al. [81, p. 2035], which was based on coating thickness measurements. The mechanisms are normally identified based on visual inspection of scanning electron microscopy images, which decreases the objectivity of the results. Furthermore, there are no compositional limits for what constitutes an alkali-, phosphorus- or silicon-rich fuel with a high

agglomeration tendency. These limits probably depend on process conditions and the combustion device to some degree, but it should be possible to give some indicative ranges based on the large research base.

There is a legitimate need in the industry for reliable agglomeration prediction methods that do not require expensive and time-consuming lab- and pilot-scale tests. To this end, the empirical prediction methods would require more comprehensive studies, where each operational parameter is changed systematically between tests. Fuel blends could be applied to get data on a wider range of ash compositions. In these studies, fuel compositions should be considered not only in terms of existing elements, but also the compounds, especially in the case of silicon. The types of ash compounds in the fuel could be identified by using chemical fractionation. The regression model used by Gatternig and Karl [35] could be improved in this way, for example.

The semi-empirical prediction methods also need more improvement. For thermochemical equilibrium calculations, experimental studies and thermodynamic evaluations should be conducted to fill the missing compositional ranges that are relevant for bed agglomeration. Computational fluid dynamics -based methods are under development and their efficiency will probably improve along with the increasing computational power available. The use of population balance and Monte Carlo methods for agglomerate growth modelling should be investigated more closely.

In the ideal case, the resulting agglomeration prediction model would also give information about the dominant agglomeration mechanism, in addition to the probability of agglomeration. This would have significance for the choice of using alternative bed materials, if they are only useful for preventing coating-induced agglomeration. The costs of different agglomeration prevention methods should also be investigated. Then, techno-economic calculations could be made about the combined use of different methods, like additives, alternative bed materials and co-combustion.

REFERENCES

[1] E. Alakangas, M. Hurskainen, J. Laatikainen-Luntama and J. Korhonen, *Suomessa käytettävien polttoaineiden ominaisuuksia*, VTT tiedotteita 2045, Teknologian tutkimuskeskus VTT Oy, Espoo, Finland, 2016, 263 p., URL: https://www.vttresearch.com/sites/default/files/pdf/technology/2016/T258.pdf.

[2] M. Almark and M. Hiltunen, *Alternative Bed Materials for High Alkali Fuels*, Proceedings of the 18th International Conference on Fluidized Bed Combustion, Toronto Ontario, Canada, 2005, 9 p., URL: https://doi.org/10.1115/FBC2005-78094.

[3] E. J. Anthony, A. P. Iribarne and J. V. Iribarne, *A New Mechanism for FBC Agglomeration and Fouling in 100 Percent Firing of Petroleum Coke*, Journal of energy resources technology, Vol. 119, No. 1, 1997, pp. 55–61, URL: https://doi.org/10.1115/1.2794223.

[4] E. Anthony and L. Jia, *Agglomeration and strength development of deposits in CFBC boilers firing high-sulfur fuels*, Fuel, Vol. 79, No. 15, 2000, pp. 1933–1942, URL: https://doi.org/10.1016/S0016-2361(00)00054-5.

[5] W. Ariyaratne, E. Manjula, C. Ratnayake and M. Melaaen, *CFD Approaches for Modeling Gas-Solids Multiphase Flows – A Review*, Proceedings of The 9th EUROSIM Congress on Modelling and Simulation, Oulu, Finland, 2016, pp. 680–686, URL: https://doi.org/10.3384/ecp17142680.

[6] R. Backman, M. Hupa and E. Uppstu, *Fouling and corrosion mechanisms in the recovery boiler superheater area*, Tappi Journal 70, 1987, pp. 123–127.

[7] R. Backman, M. Hupa and B.-J. Skrifvars, *Predicting Superheater Deposit Formation in Boilers Burning Biomasses*, *In: Impact of Mineral Impurities in Solid Fuel Combustion*, ed. by R. P. Gupta, T. F. Wall and L. Baxter, Springer, Boston Massachusetts, USA, 1999, pp. 405–416, URL: https://doi.org/10.1007/0-306-46920-0_30.

[8] B. V. Balakin, S. Alyaev, A. C. Hoffmann and P. Kosinski, *Micromechanics of agglomeration forced by the capillary bridge: The restitution of momentum*, AIChE Journal, Vol. 59, No. 11, 2013, pp. 4045–4057, URL: https://doi.org/10.1002/aic.14162.

[9] B. V. Balakin, K. V. Kutsenko, A. A. Lavrukhin and P. Kosinski, *The collision efficiency of liquid bridge agglomeration*, Chemical Engineering Science, Vol. 137, 2015, pp. 590–600, URL: https://doi.org/10.1016/j.ces.2015.07.002.

[10] M. Balland, K. Froment, G. Ratel, S. Valin, J. Roussely, R. Michel, J. Poirier, Y. Kara and A. Galnares, *Biomass Ash Fluidised-Bed Agglomeration: Hydrodynamic Investigations*, Waste and Biomass Valorization, Vol. 8, No. 8, 2017, pp. 2823–2841, URL: https://doi.org/10.1007/s12649-017-9853-9.

[11] V. Barisic, E. Coda Zabetta and L.-E. Åmand, *The Role of Limestone in Preventing Agglomeration and Slagging during CFB Combustion of High-Phosphorous Fuels*, Proceedings Poster Session for World BioEnergy 2008 Conference & Exhibition on Biomass for Energy, Jönköping, Sweden, 2008, pp. 259–263, URL: https://research.chalmers.se/en/publication/237436.

[12] M. Bartels, W. Lin, J. Nijenhuis, F. Kapteijn and J. R. van Ommen, *Agglomeration in fluidized beds at high temperatures: Mechanisms, detection and prevention*, Progress in energy and combustion science, Vol. 34, No. 5, 2008, pp. 633–666, URL: https://doi.org/10.1016/j.pecs.2008.04.002.

[13] P. Billen, J. Van Caneghem and C. Vandecasteele, *Predicting Melt Formation and Agglomeration in Fluidized Bed Combustors by Equilibrium Calculations*, Waste and Biomass Valorization, Vol. 5, No. 5, 2014, pp. 879–892, URL: http://doi.org/10.1007/s12649-013-9285-0.

[14] D. Boström, N. Skoglund, A. Grimm, C. Boman, M. Öhman, M. Broström and R. Backman, *Ash Transformation Chemistry during Combustion of Biomass*, Energy & Fuels, Vol. 26, No. 1, 2012, pp. 85–93, URL: https://doi.org/10.1021/ef201205b.

[15] C. Boyce, *Gas-solid fluidization with liquid bridging: A review from a modeling perspective*, Powder Technology, Vol. 336, 2018, pp. 12–29, URL: https://doi.org/10.1016/j.powtec.2018.05.027.

[16] E. Brus, M. Öhman and A. Nordin, *Mechanisms of Bed Agglomeration during Fluidized-Bed Combustion of Biomass Fuels*, Energy & Fuels, Vol. 19, No. 3, 2005, pp. 825–832, URL: https://doi.org/10.1021/ef0400868.

[17] E. Brus, M. Öhman, A. Nordin, D. Boström, H. Hedman and A. Eklund, *Bed Agglomeration Characteristics of Biomass Fuels Using Blast-Furnace Slag as Bed Material*, Energy & Fuels, Vol. 18, No. 4, 2004, pp. 1187–1193, URL: https://doi.org/10.1021/ef034095c.

[18] E. Brus, M. Öhman, A. Nordin, B.-J. Skrifvars and R. Backman, *Bed Material Consumption in Biomass Fired Fluidised Bed Boilers Due to Risk of Bed Agglomeration - Coating Formation and Possibilities for Regeneration*, IFRF Combustion Journal, Article Number 200302, 2003, 12 p., URL: https://ifrf.net/research/archive/bed-material-consumption-in-biomass-fired-fluidised-bed-boilers-due-to-risk-of-bed-agglomeration-coating-formation-and-possibilities-for-regeneration/.

[19] R. W. Bryers, *Fireside slagging, fouling, and high-temperature corrosion of heat-transfer surface due to impurities in steam-raising fuels*, Progress in energy and combustion science, Vol. 22, No. 1, 1996, pp. 29–120, URL: https://doi.org/10.1016/0360-1285(95)00012-7.

[20] CAIT Climate Data Explorer, *Country Greenhouse Gas Emissions*, World Resources Institute, 2016, URL: https://www.climatewatchdata.org/ghg-emissions (accessed on 13.8.2020).

[21] W. D. Callister and D. G. Rethwisch, *Materials science and engineering*, 8th ed., Wiley, Hoboken New Jersey, USA, 2010, 885 p.

[22] C. B. Carter and M. G. Norton, *Ceramic Materials: Science and Engineering*, Springer, New York, USA, 2013, 766 p.

[23] T. Chai and R. R. Draxler, *Root mean square error (RMSE) or mean absolute error (MAE)? – Arguments against avoiding RMSE in the literature*, Geoscientific model development, Vol. 7, No. 3, 2014, pp. 1247–1250, URL: https://doi.org/10.5194/gmd-7-1247-2014.

[24] P. Chaivatamaset, P. Sricharoon and S. Tia, *Bed agglomeration characteristics of palm shell and corncob combustion in fluidized bed*, Applied thermal engineering, Vol. 31, No. 14-15, 2011, pp. 2916–2927, URL: https://doi.org/10.1016/j.applthermaleng.2011.05.021.

[25] P. Chaivatamaset, P. Sricharoon, S. Tia and B. Bilitewski, *The characteristics of bed agglomeration/defluidization in fluidized bed firing palm fruit bunch and rice straw*, Applied thermal engineering, Vol. 70, No. 1, 2014, pp. 737–747, URL: https://doi.org/10.1016/j.applthermaleng.2014.05.061.

[26] R. Chirone, F. Miccio and F. Scala, *Mechanism and prediction of bed agglomeration during fluidized bed combustion of a biomass fuel: Effect of the reactor scale*, Chemical engineering journal, Vol. 123, No. 3, 2006, pp. 71–80, URL: https://doi.org/10.1016/j.cej.2006.07.004.

[27] R. Chirone, P. Salatino and F. Scala, *The relevance of attrition to the fate of ashes during fluidized-bed combustion of a biomass*, Proceedings of the Combustion Institute, Vol. 28, No. 2, 2000, pp. 2279–2286, URL: https://doi.org/10.1016/S0082-0784(00)80638-4.

[28] P. Darabi, K. Pougatch, M. Salcudean and D. Grecov, *A novel coalescence model for binary collision of identical wet particles*, Chemical Engineering Science, Vol. 64, No. 8, 2009, pp. 1868–1876, URL: https://doi.org/10.1016/j.ces.2009.01.017.

[29] K. Davidsson, L.-E. Åmand, B.-M. Steenari, A.-L. Elled, D. Eskilsson and B. Leckner, *Countermeasures against alkali-related problems during combustion of biomass in a circulating fluidized bed boiler*, Chemical Engineering Science, Vol. 63, No. 21, 2008, pp. 5314–5329, URL: https://doi.org/10.1016/j.ces.2008.07.012.

[30] S. De Geyter, M. Öhman, D. Boström, M. Eriksson and A. Nordin, *Effects of Non-Quartz Minerals in Natural Bed Sand on Agglomeration Characteristics during Fluidized Bed Combustion of Biomass Fuels*, Energy & Fuels, Vol. 21, No. 5, 2007, pp. 2663–2668, URL: https://doi.org/10.1021/ef070162h.

[31] S. De Geyter, M. Öhman, M. Eriksson, A. Nordin, D. Boström and M. Berg, *Agglomeration characteristics using alternative bed materials for combustion of biomass*, Proceedings of the 14th European Biomass Conference, Paris, France, 2005, pp. 1343–1346, URL: https://www.diva-portal.org/smash/get/diva2:1007779/FULLTEXT01.pdf.

[32] F. Dijen, P. Savat, J. Vanormelingen and H. Sablon, *Ultra supercritical pulverised fuel combustion versus ultra supercritical circulating fluidised bed combustion: Is ultra supercritical circulating fluidised bed combustion on top?*, VGB PowerTech, Vol. 85, No. 11, 2005, pp. 64–66.

[33] J. Drake, *Hydrodynamic Characterization of 3D Fluidized Beds Using Noninvasive Techniques*, Iowa State University, Graduate Theses and Dissertations 10313, 2011, p. 194, URL: https://doi.org/10.31274/etd-180810-2256.

[34] A.-L. Elled, L.-E. Åmand and B.-M. Steenari, *Composition of agglomerates in fluidized bed reactors for thermochemical conversion of biomass and waste fuels Experimental data in comparison with predictions by a thermodynamic equilibrium model*, Fuel, Vol. 111, 2013, pp. 696–708, URL: https://doi.org/10.1016/j.fuel.2013.03.018.

[35] B. Gatternig and J. Karl, *Prediction of ash-induced agglomeration in biomass-fired fluidized beds by an advanced regression-based approach*, Fuel, Vol. 161, 2015, pp. 157–167, URL: https://doi.org/10.1016/j.fuel.2015.08.040.

[36] B. Gatternig, *Predicting Agglomeration in Biomass Fired Fluidized Beds*, PhD Dissertation, Friedrich-Alexander-University of Erlangen-Nürnberg, 2015, 188 p., URL: http://nbn-resolving.de/urn:nbn:de:bvb:29-opus4-62359.

[37] B. Gatternig and J. Karl, *A discrete element cohesive particle collision model for the prediction of ash-induced agglomeration*, International journal of ambient energy, 2019, pp. 1–9, URL: https://doi.org/10.1080/01430750.2019.1594367.

[38] B. Gatternig and J. Karl, *Application of chemical equilibrium calculations for the prediction of ash-induced agglomeration*, Biomass Conversion and Biorefinery, Vol. 9, No. 1, 2018, pp. 117–128, URL: https://doi.org/10.1007/s13399-018-0325-7.

[39] B. Gatternig and J. Karl, *Investigations on the Mechanisms of Ash-Induced Agglomeration in Fluidized-Bed Combustion of Biomass*, Energy & Fuels, Vol. 29, No. 2, 2015, pp. 931–941, URL: https://doi.org/10.1021/ef502658b.

[40] B. Gatternig and J. Karl, *The Influence of Particle Size, Fluidization Velocity, and Fuel Type on Ash-Induced Agglomeration in Biomass Combustion*, Frontiers in energy research, Vol. 2, 2014, URL: https://doi.org/10.3389/fenrg.2014.00051.

[41] D. Geldart, *Types of gas fluidization*, Powder technology, Vol. 7, No. 5, 1973, pp. 285–292, URL: https://doi.org/10.1016/0032-5910(73)80037-3.

[42] P. Glarborg and P. Marshall, *Mechanism and modeling of the formation of gaseous alkali sulfates*, Combustion and Flame, Vol. 141, No. 1, 2005, pp. 22–39, URL: https://doi.org/10.1016/j.combustflame.2004.08.014.

[43] M. J. Gluckman, Y. J. and A. M. Squires, *Defluidization Characteristics of Sticky or Agglomerating Beds*, *In: Fluidization Technology, Vol II*, ed. by D. L. Keairns, Hemisphere, Washington, DC, USA, 1976, pp. 395–422.

[44] P. Grammelis, *Solid Biofuels for Energy - A Lower Greenhouse Gas Alternative*, 1st ed., Springer, London, UK, 2011, 242 p., URL: https://doi-org.libproxy.tuni.fi/10.1007/978-1-84996-393-0.

[45] A. Grimm, M. Öhman, T. Lindberg, A. Fredriksson and D. Boström, *Bed Agglomeration Characteristics in Fluidized-Bed Combustion of Biomass Fuels Using Olivine as Bed Material*, Energy & Fuels, Vol. 26, No. 7, 2012, pp. 4550–4559, URL: https://doi.org/10.1021/ef300569n.

[46] A. Grimm, N. Skoglund, D. Boström and M. Öhman, *Bed Agglomeration Characteristics in Fluidized Quartz Bed Combustion of Phosphorus-Rich Biomass Fuels*, Energy & Fuels, Vol. 25, No. 3, 2011, pp. 937–947, URL: https://doi.org/10.1021/ef101451e.

[47] N. G. Halford and A. Karp, *Energy crops*, Royal Society of Chemistry, Cambridge, UK, 2010, 443 p.

[48] H. He, D. Boström and M. Öhman, *Time Dependence of Bed Particle Layer Formation in Fluidized Quartz Bed Combustion of Wood-Derived Fuels*, Energy & Fuels, Vol. 28, No. 6, 2014, pp. 3841–3848, URL: https://doi.org/10.1021/ef500386k.

[49] H. He, X. Ji, D. Boström, R. Backman and M. Öhman, *Mechanism of Quartz Bed Particle Layer Formation in Fluidized Bed Combustion of Wood-Derived Fuels*, Energy & Fuels, Vol. 30, No. 3, 2016, pp. 2227–2232, URL: https://doi.org/10.1021/acs.energyfuels.5b02891.

[50] H. He, N. Skoglund and M. Öhman, *Time-Dependent Crack Layer Formation in Quartz Bed Particles during Fluidized Bed Combustion of Woody Biomass*, Energy & Fuels, Vol. 31, No. 2, 2017, pp. 1672–1677, URL: https://doi.org/10.1021/acs.energyfuels.6b02980.

[51] M. Hupa, *Ash-Related Issues in Fluidized-Bed Combustion of Biomasses: Recent Research Highlights*, Energy & Fuels, Vol. 26, No. 1, 2012, pp. 4–14, URL: https://doi.org/10.1021/ef201169k.

[52] IPCC, *Renewable energy sources and climate change mitigation: special report of the Intergovernmental Panel on Climate Change*, Cambridge University Press, New York, USA, 2012, 1088 p., URL: https://www.ipcc.ch/report/renewable-energy-sources-and-climate-change-mitigation/.

[53] IPCC, *Summary for Policymakers. In: Global Warming of 1.5 °C. An IPCC Special Report on the impacts of global warming of 1.5 °C above pre-industrial levels and related global greenhouse gas emission pathways, in the context of strengthening the global response to the threat of climate change, sustainable development, and efforts to eradicate poverty*, 2018, URL: https://www.ipcc.ch/sr15/chapter/spm/.

[54] B. Jenkins, L. Baxter and T. Miles, *Combustion properties of biomass*, Fuel processing technology, Vol. 54, No. 1-3, 1998, pp. 17–46, URL: https://doi.org/10.1016/S0378-3820(97)00059-3.

[55] A. B. Khadilkar, P. L. Rozelle and S. V. Pisupati, *Investigation of fluidized bed agglomerate growth process using simulations and SEM-EDX characterization of laboratory-generated agglomerates*, Chemical Engineering Science, Vol. 184, 2018, pp. 172–185, URL: https://doi.org/10.1016/j.ces.2018.03.035.

[56] A. B. Khadilkar, P. L. Rozelle and S. V. Pisupati, *Review of Particle Physics and Chemistry in Fluidized Beds for Development of Comprehensive Ash Agglomeration Prediction Models*, Energy & Fuels, Vol. 30, No. 5, 2016, pp. 3714–3734, URL: https://doi.org/10.1021/acs.energyfuels.6b00079.

[57] A. Khadilkar, P. L. Rozelle and S. V. Pisupati, *Models of agglomerate growth in fluidized bed reactors: Critical review, status and applications*, Powder Technology, Vol. 264, 2014, pp. 216–228, URL: https://doi.org/10.1016/j.powtec.2014.04.063.

[58] A. Khan, *Combustion and co-combustion of biomass in a bubbling fluidized bed boiler*, PhD Dissertation, Delft University of Technology, 2007, 190 p., URL: https://repository.tudelft.nl/islandora/object/uuid%5C%3Ad0e9adab-acea-425e-85a3-3722f285a1c4.

[59] A. Khan, W. de Jong, P. Jansens and H. Spliethoff, *Biomass combustion in fluidized bed boilers: Potential problems and remedies*, Fuel processing technology, Vol. 90, No. 1, 2009, pp. 21–50, URL: https://doi.org/10.1016/j.fuproc.2008.07.012.

[60] T. Kittivech and S. Fukuda, *Effect of Bed Material on Bed Agglomeration for Palm Empty Fruit Bunch (EFB) Gasification in a Bubbling Fluidised Bed System*, Energies, Vol. 12, 2019, pp. 1–16, URL: https://doi.org/10.3390/en12224336.

[61] J. Kitto and S. Stultz, *Steam: its generation and use. 41st edition. Chapter 17: Fluidized-Bed Combustion*, The Babcock & Wilcox Company, Barberton Ohio, USA, 2005, 16 p.

[62] P. Knutsson, G. Schwebel, B.-M. Steenari and H. Leion, *Effect of bed materials mixing on the observed bed sintering*, Proceedings of the 11th International Conference on Fluidized Bed Technology, Beijing, China, 2014, pp. 655–660, URL: https://research.chalmers.se/publication/200334.

[63] R. Korbee, J. Lensselink, J. v. Ommen, J. Nijenhuis, M. v. Gemert and K. Haasnoot, *Early Agglomeration Recognition System - EARS: From bench-scale testing to industrial prototype*, ECN project 7.2260, The Energy Research Centre of the Netherlands, 2004, 51 p.

[64] R. Korbee, J. van Ommen, J. Lensselink, J. Nijenhuis, J. Kiel and C. van den Bleek, *Early Agglomeration Recognition System (EARS)*, Journal of energy resources technology, Vol. 128, No. 2, 2006, pp. 143–149, URL: https://doi.org/10.1115/1.2191505.

[65] N. Kumar, P. Besuner, S. Lefton, D. Agan and D. Hilleman, *Power Plant Cycling Costs*, National Renewable Energy Laboratory (U.S.), Golden Colorado, USA, 2012, 83 p., URL: https://doi.org/10.2172/1046269.

[66] W. Lin, K. Dam-Johansen and F. Frandsen, *Agglomeration in bio-fuel fired fluidized bed combustors*, Chemical Engineering Journal, Vol. 96, No. 1, 2003, pp. 171–185, URL: https://doi.org/10.1016/j.cej.2003.08.008.

[67] D. Lindberg, R. Backman, P. Chartrand and M. Hupa, *Towards a comprehensive thermodynamic database for ash-forming elements in biomass and waste combustion – Current situation and future developments*, Fuel Processing Technology, Vol. 105, 2013, pp. 129–141, URL: https://doi.org/10.1016/j.fuproc.2011.08.008.

[68] E. Lindström, M. Sandström, D. Boström and M. Öhman, *Slagging Characteristics during Combustion of Cereal Grains Rich in Phosphorus*, Energy & Fuels, Vol. 21, No. 2, 2007, pp. 710–717, URL: https://doi.org/10.1021/ef060429x.

[69] H. Liu, Y. Feng, S. Wu and D. Liu, *The role of ash particles in the bed agglomeration during the fluidized bed combustion of rice straw*, Bioresource Technology, Vol. 100, No. 24, 2009, pp. 6505–6513, URL: https://doi.org/10.1016/j.biortech.2009.06.098.

[70] B. G. Miller and D. A. Tillman, *Combustion Engineering Issues for Solid Fuel Systems*, Elsevier Inc., 2008, 528 p., URL: https://doi.org/10.1016/B978-0-12-373611-6.X0001-8.

[71] G. W. Morey, *The Binary Systems $NaPO_3$-KPO_3 and $K_4P_2O_7$-KPO_3*, Journal of the American Chemical Society, Vol. 76, No. 18, 1954, pp. 4724–4726, URL: https://doi.org/10.1021/ja01647a069.

[72] J. D. Morris, S. S. Daood, S. Chilton and W. Nimmo, *Mechanisms and mitigation of agglomeration during fluidized bed combustion of biomass: A review*, Fuel, Vol. 230, 2018, pp. 452–473, URL: https://doi.org/10.1016/j.fuel.2018.04.098.

[73] L. H. Nuutinen, M. S. Tiainen, M. E. Virtanen, S. H. Enestam and R. S. Laitinen, *Coating Layers on Bed Particles during Biomass Fuel Combustion in Fluidized-Bed Boilers*, Energy & Fuels, Vol. 18, No. 1, 2004, pp. 127–139, URL: https://doi.org/10.1021/ef0300850.

[74] M. Öhman and A. Nordin, *Review of particle temperature studies in fluidized bed combustion*, Proceedings of the Nordic seminar on thermochemical conversion of solid fuels, Trondheim, Norway, 1996, 11 p., URL: http://urn.kb.se/resolve?urn=urn:nbn:se:ltu:diva-35573.

[75] M. Öhman and A. Nordin, *A New Method for Quantification of Fluidized Bed Agglomeration Tendencies: A Sensitivity Analysis*, Energy & Fuels, Vol. 12, No. 1, 1998, pp. 90–94, URL: https://doi.org/10.1021/ef970049z.

[76] M. Öhman and A. Nordin, *The Role of Kaolin in Prevention of Bed Agglomeration during Fluidized Bed Combustion of Biomass Fuels*, Energy & Fuels, Vol. 14, No. 3, 2000, pp. 618–624, URL: https://doi.org/10.1021/ef990198c.

[77] M. Öhman, A. Nordin, B.-J. Skrifvars, R. Backman and M. Hupa, *Bed Agglomeration Characteristics during Fluidized Bed Combustion of Biomass Fuels*, Energy & Fuels, Vol. 14, No. 1, 2000, pp. 169–178, URL: https://doi.org/10.1021/ef990107b.

[78] M. Öhman, L. Pommer and A. Nordin, *Bed Agglomeration Characteristics and Mechanisms during Gasification and Combustion of Biomass Fuels*, Energy & Fuels, Vol. 19, No. 4, 2005, pp. 1742–1748, URL: https://doi.org/10.1021/ef040093w.

[79] G. Olofsson, Z. Ye, I. Bjerle and A. Andersson, *Bed Agglomeration Problems in Fluidized-Bed Biomass Combustion*, Industrial & Engineering Chemistry Research, Vol. 41, No. 12, 2002, pp. 2888–2894, URL: https://doi.org/10.1021/ie010274a.

[80] P. Pagliai, S. Simons and D. Rhodes, *Towards a fundamental understanding of defluidisation at high temperatures: a micro-mechanistic approach*, Powder Technology, Vol. 148, No. 2, 2004, pp. 106–112, URL: https://doi.org/10.1016/j.powtec.2004.09.004.

[81] P. Piotrowska, A. Grimm, N. Skoglund, C. Boman, M. Öhman, M. Zevenhoven, D. Boström and M. Hupa, *Fluidized-Bed Combustion of Mixtures of Rapeseed Cake and Bark: The Resulting Bed Agglomeration Characteristics*, Energy & Fuels, Vol. 26, No. 4, 2012, pp. 2028–2037, URL: https://doi.org/10.1021/ef300130e.

[82] P. Piotrowska, M. Zevenhoven, K. Davidsson, M. Hupa, L.-E. Åmand, V. Barišić and E. Coda Zabetta, *Fate of Alkali Metals and Phosphorus of Rapeseed Cake in Circulating Fluidized Bed Boiler Part 1: Cocombustion with Wood*, Energy & fuels, Vol. 24, No. 1, 2010, pp. 333–345, URL: https://doi.org/10.1021/ef900822u.

[83] O. Pitois, P. Moucheront and X. Chateau, *Liquid Bridge between Two Moving Spheres: An Experimental Study of Viscosity Effects*, Journal of colloid and interface science, Vol. 231, No. 1, 2000, pp. 26–31, URL: https://doi.org/10.1006/jcis.2000.7096.

[84] M. N. Rahaman, *Ceramic Processing and Sintering*, 2nd ed., Marcel Dekker, New York, USA, 2017, 875 p.

[85] R. Raiko, J. Saastamoinen, M. Hupa and I. Kurki-Suonio, *Poltto ja palaminen*, 2. täydennetty painos, International Flame Research Foundation – Suomen kansallinen osasto, Jyväskylä, Finland, 2002, 750 p.

[86] S. T. Raji T. O. Oyewola O.M., *New features for performance enhancement of experimental Model Bubbling Fluidized Bed Combustor*, International Journal of Scientific & Engineering Research, Vol. 3, No. 1, 2012, pp. 1–10, URL: https://www.ijser.org/paper/New-features-for-performance-enhancement-of-experimental-Model-Bubbling-Fluidized-Bed-Combustor.html.

[87] W. T. Reid, *The relation of mineral composition to slagging, fouling and erosion during and after combustion*, Progress in Energy and Combustion Science, Vol. 10, No. 2, 1984, pp. 159–169, URL: https://doi.org/10.1016/0360-1285(84)90100-X.

[88] D. W. Richerson, *Modern ceramic engineering : properties, processing and use in design*, Marcel Dekker, New York, USA, 1982, 399 p.

[89] E. Roedder, *Silicate melt systems*, Physics and Chemistry of the Earth, Vol. 3, 1959, pp. 224–297, URL: https://doi.org/10.1016/0079-1946(59)90007-2.

[90] L. Rosendahl, *Biomass combustion science, technology and engineering*, Woodhead Publishing Limited, Cambridge, UK, 2013, 320 p.

[91] F. Scala, *Fluidized bed technologies for near-zero emission combustion and gasification*, Woodhead Publishing, Philadelphia Pennsylvania, USA, 2013, 1091 p.

[92] F. Scala and R. Chirone, *An SEM/EDX study of bed agglomerates formed during fluidized bed combustion of three biomass fuels*, Biomass and Bioenergy, Vol. 32, No. 3, 2008, pp. 252–266, URL: https://doi.org/10.1016/j.biombioe.2007.09.009.

[93] F. Scala and R. Chirone, *Characterization and Early Detection of Bed Agglomeration during the Fluidized Bed Combustion of Olive Husk*, Energy & Fuels, Vol. 20, No. 1, 2006, pp. 120–132, URL: https://doi.org/10.1021/ef050236u.

[94] F. Scala, R. Chirone and P. Salatino, *The influence of fine char particles burnout on bed agglomeration during the fluidized bed combustion of a biomass fuel*, Fuel processing technology, Vol. 84, No. 1, 2003, pp. 229–241, URL: https://doi.org/10.1016/S0378-3820(03)00108-5.

[95] C. L. Senior and S. Srinivasachar, *Viscosity of Ash Particles in Combustion Systems for Prediction of Particle Sticking*, Energy & Fuels, Vol. 9, No. 2, 1995, pp. 277–283, URL: https://doi.org/10.1021/ef00050a010.

[96] J. Seville, C. Willett and P. Knight, *Interparticle forces in fluidisation: a review*, Powder technology, Vol. 113, No. 3, 2000, pp. 261–268, URL: https://doi.org/10.1016/S0032-5910(00)00309-0.

[97] J. Shabanian, M. A. Duchesne, A. Runstedtler, M. Syamlal and R. W. Hughes, *Improved analytical energy balance model for evaluating agglomeration from a binary collision of identical wet particles*, Chemical engineering science, Vol. 223, 2020, pp. 1–20, URL: https://doi.org/10.1016/j.ces.2020.115738.

[98] J. Shabanian, R. Jafari and J. Chaouki, *Fluidization of ultrafine powders*, International Review of Chemical Engineering, Vol. 4, No. 1, 2012, pp. 16–50, URL: https://www.researchgate.net/publication/270959459_Fluidization_of_ultrafine_powders.

[99] J. Silvennoinen, *A New Method to Inhibit Bed Agglomeration Problems in Fluidized Bed Boilers*, Proceedings of the 17th International Fluidized Bed Combustion Conference, Jacksonville Florida, USA, 2003, pp. 1–9, URL: https://doi.org/10.1115/FBC2003-081.

[100] B.-J. Skrifvars, M. Hupa and E. J. Anthony, *Mechanisms of Bed Material Agglomeration in a Petroleum Coke-Fired Circulating Fluidized Bed Boiler*, Journal of energy resources technology, Vol. 120, No. 3, 1998, pp. 215–218, URL: https://doi.org/10.1115/1.2795038.

[101] B.-J. Skrifvars, R. Backman and M. Hupa, *Characterization of the sintering tendency of ten biomass ashes in FBC conditions by a laboratory test and by phase equilibrium calculations*, Fuel Processing Technology, Vol. 56, No. 1, 1998, pp. 55–67, URL: https://doi.org/10.1016/S0378-3820(97)00084-2.

[102] B.-J. Skrifvars, M. Hupa, R. Backman and M. Hiltunen, *Sintering mechanisms of FBC ashes*, Fuel, Vol. 73, No. 2, 1994, pp. 171–176, URL: https://doi.org/10.1016/0016-2361(94)90110-4.

[103] H. Spliethoff, *Power generation from solid fuels*, Springer, Berlin, Germany, 2010, 672 p.

[104] B.-M. Steenari and O. Lindqvist, *High-temperature reactions of straw ash and the anti-sintering additives kaolin and dolomite*, Biomass and Bioenergy, Vol. 14, No. 1, 1998, pp. 67–76, URL: https://doi.org/10.1016/S0961-9534(97)00035-4.

[105] B.-M. Steenari, A. Lundberg, H. Pettersson, M. Wilewska-Bien and D. Andersson, *Investigation of Ash Sintering during Combustion of Agricultural Residues and the Effect of Additives*, Energy & Fuels, Vol. 23, No. 11, 2009, pp. 5655–5662, URL: https://doi.org/10.1021/ef900471u.

[106] P. Thy, B. Jenkins, R. Williams, C. Lesher and R. Bakker, *Bed agglomeration in fluidized combustor fueled by wood and rice straw blends*, Fuel Processing Technology, Vol. 91, No. 11, 2010, pp. 1464–1485, URL: https://doi.org/10.1016/j.fuproc.2010.05.024.

[107] P. Thy, C. Lesher and B. Jenkins, *Experimental determination of high-temperature elemental losses from biomass slag*, Fuel, Vol. 79, No. 6, 2000, pp. 693–700, URL: https://doi.org/10.1016/S0016-2361(99)00195-7.

[108] E. K. Vakkilainen, *Steam Generation from Biomass - Construction and Design of Large Boilers*, Elsevier, 2017, 322 p., URL: https://app.knovel.com/hotlink/toc/id:kpSGBCDLBC/steam-generation-from/steam-generation-from.

[109] S. Vargas, F. Frandsen and K. Dam-Johansen, *Rheological properties of high-temperature melts of coal ashes and other silicates*, Progress in Energy and Combustion Science, Vol. 27, No. 3, 2001, pp. 237–429, URL: https://doi.org/10.1016/S0360-1285(00)00023-X.

[110] S. V. Vassilev, D. Baxter and C. G. Vassileva, *An overview of the behaviour of biomass during combustion: Part II. Ash fusion and ash formation mechanisms of biomass types*, Fuel, Vol. 117, 2014, pp. 152–183, URL: https://doi-org.libproxy.tuni.fi/10.1016/j.fuel.2013.09.024.

[111] S. V. Vassilev, C. G. Vassileva, Y.-C. Song, W.-Y. Li and J. Feng, *Ash contents and ash-forming elements of biomass and their significance for solid biofuel combustion*, Fuel, Vol. 208, 2017, pp. 377–409, URL: https://doi.org/10.1016/j.fuel.2017.07.036.

[112] H. Visser, *The influence of fuel composition on agglomeration behaviour in fluidised bed combustion*, ECN project 7.2258, the Energy Research Centre of the Netherlands, 2004, 44 p., URL: https://www.researchgate.net/publication/265493933_The_influence_of_fuel_composition_on_agglomeration_behaviour_in_fluidised_bed_combustion.

[113] H. J. M. Visser, S. C. van Lith and J. H. A. Kiel, *Biomass Ash-Bed Material Interactions Leading to Agglomeration in FBC*, Journal of energy resources technology, Vol. 130, No. 1, 2008, pp. 1–6, URL: https://doi.org/10.1115/1.2824247.

[114] H. Visser, H. Hofmans, H. Huijnen, R. Kastelein and J. Kiel, *Biomass Ash – Bed Material Interactions Leading to Agglomeration in Fluidised Bed Combustion and Gasification*, Blackwell Science Ltd, Oxford, UK, 2001, pp. 272–286, URL: https://doi.org/10.1002/9780470694954.ch20.

[115] H. Visser, van Lith S.C. and J. H. A. Kiel, *Biomass ash - bed material interactions leading to agglomeration in FBC*, Proceedings of the 17th International Fluidized Bed Combustion Conference, Jacksonville Florida, USA, 2003, pp. 1–8.

[116] J. Visser, *Van der Waals and other cohesive forces affecting powder fluidization*, Powder technology, Vol. 58, No. 1, 1989, pp. 1–10, URL: https://doi.org/10.1016/0032-5910(89)80001-4.

[117] K. Wagner, G. Häggström, N. Skoglund, J. Priscak, M. Kuba, M. Öhman and H. Hofbauer, *Layer formation mechanism of K-feldspar in bubbling fluidized bed combustion of phosphorus-lean and phosphorus-rich residual biomass*, Applied energy, Vol. 248, 2019, pp. 545–554, URL: https://doi.org/10.1016/j.apenergy.2019.04.112.

[118] L. Wang, J. E. Hustad, Ø. Skreiberg, G. Skjevrak and M. Grønli, *A Critical Review on Additives to Reduce Ash Related Operation Problems in Biomass Combustion Applications*, Energy procedia, Vol. 20, 2012, pp. 20–29, URL: https://doi.org/10.1016/j.egypro.2012.03.004.

[119] J. Werther, M. Saenger, E.-U. Hartge, T. Ogada and Z. Siagi, *Combustion of agricultural residues*, Progress in energy and combustion science, Vol. 26, No. 1, 2000, pp. 1–27, URL: https://doi.org/10.1016/S0360-1285(99)00005-2.

[120] J. Werther, *Measurement techniques in fluidized beds*, Powder Technology, Vol. 102, No. 1, 1999, pp. 15–36, URL: https://doi.org/10.1016/S0032-5910(98)00202-2.

[121] A. Williams, M. Pourkashanian and J. Jones, *Combustion of pulverised coal and biomass*, Progress in energy and combustion science, Vol. 27, No. 6, 2001, pp. 587–610, URL: https://doi.org/10.1016/S0360-1285(01)00004-1.

[122] C. Yu, J. Qin, H. Nie, M. Fang and Z. Luo, *Experimental research on agglomeration in straw-fired fluidized beds*, Applied Energy, Vol. 88, No. 12, 2011, pp. 4534–4543, URL: https://doi.org/10.1016/j.apenergy.2011.05.046.

[123] M. Zevenhoven-Onderwater, M. Öhman, B.-J. Skrifvars, R. Backman, A. Nordin and M. Hupa, *Bed Agglomeration Characteristics of Wood-Derived Fuels in FBC*, Energy & Fuels, Vol. 20, No. 2, 2006, pp. 818–824, URL: https://doi.org/10.1021/ef050349d.

[124] M. Zevenhoven, B.-J. Skrifvars, P. Yrjas, M. Hupa, L. Nuutinen and R. Laitinen, *Searching for improved characterization of ash forming matter in biomass*, Proceedings of the 16th International Conference on Fluidized Bed Combustion, Reno Nevada, USA, 2001, 18 p.

[125] M. Zevenhoven, P. Yrjas and M. Hupa, *Ash-Forming Matter and Ash-Related Problems*, *In: Handbook of Combustion Vol. 4: Solid Fuels*, Wiley, 2010, pp. 493–531, URL: https://doi.org/10.1002/9783527628148.hoc068.

[126] M. Zevenhoven, P. Yrjas, B.-J. Skrifvars and M. Hupa, *Characterization of Ash-Forming Matter in Various Solid Fuels by Selective Leaching and Its Implications for Fluidized-Bed Combustion*, Energy & Fuels, Vol. 26, No. 10, 2012, pp. 6366–6386, URL: https://doi.org/10.1021/ef300621j.

[127] Y. Zhang, Q. Li and H. Zhou, *Theory and calculation of heat transfer in furnaces*, Elsevier, 2016, 447 p.

[128] H. Zhu, Z. Zhou, R. Yang and A. Yu, *Discrete particle simulation of particulate systems: Theoretical developments*, Chemical engineering science, Vol. 62, No. 13, 2007, pp. 3378–3396, URL: https://doi.org/10.1016/j.ces.2006.12.089.

[129] S. S. Zumdahl and S. A. Zumdahl, *Chemistry, 7th edition*, Houghton Mifflin Company, Boston Massachusetts, USA, 2007, 1056 p.